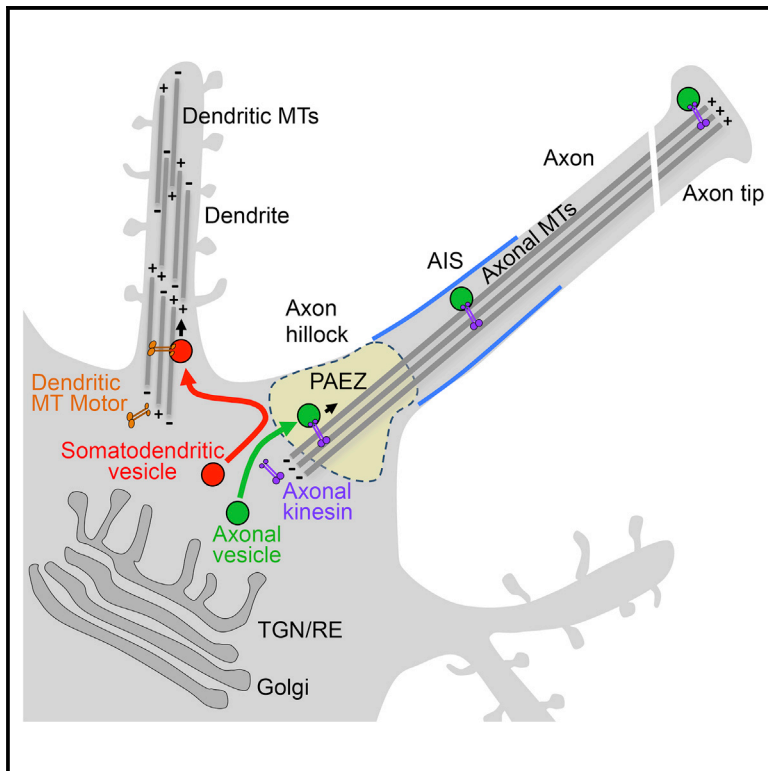


Sorting of Dendritic and Axonal Vesicles at the Pre-axonal Exclusion Zone

Graphical Abstract



Authors

Ginny G. Farías, Carlos M. Guardia,
Dylan J. Britt, Xiaoli Guo,
Juan S. Bonifacino

Correspondence

bonifacinoj@helix.nih.gov

In Brief

Farías et al. show that sorting of vesicular transport carriers to the somatodendritic and axonal domains of neurons occurs at a pre-axonal exclusion zone (PAEZ) located in the axon hillock. Sorting at the PAEZ is proposed to involve differential binding of the carriers to specific microtubule motors.

Highlights

- We define a neuronal region named the pre-axonal exclusion zone (PAEZ)
- Somatodendritic vesicles are excluded from the axon at the PAEZ
- Coupling to an axonal kinesin overcomes vesicle exclusion at the PAEZ
- Polarized sorting at the PAEZ depends on differential binding to microtubule motors



Sorting of Dendritic and Axonal Vesicles at the Pre-axonal Exclusion Zone

Ginny G. Fariás,¹ Carlos M. Guardia,¹ Dylan J. Britt,¹ Xiaoli Guo,¹ and Juan S. Bonifacino^{1,*}¹Cell Biology and Metabolism Program, Eunice Kennedy Shriver National Institute of Child Health and Human Development (NICHD), NIH, Bethesda, MD 20892, USA*Correspondence: bonifacinoj@helix.nih.gov<http://dx.doi.org/10.1016/j.celrep.2015.09.074>This is an open access article under the CC BY-NC-ND license (<http://creativecommons.org/licenses/by-nc-nd/4.0/>).

SUMMARY

Polarized sorting of newly synthesized proteins to the somatodendritic and axonal domains of neurons occurs by selective incorporation into distinct populations of vesicular transport carriers. An unresolved issue is how the vesicles themselves are sorted to their corresponding neuronal domains. Previous studies concluded that the axon initial segment (AIS) is an actin-based filter that selectively prevents passage of somatodendritic vesicles into the axon. We find, however, that most somatodendritic vesicles fail to enter the axon at a more proximal region in the axon hillock, herein referred to as the pre-axonal exclusion zone (PAEZ). Forced coupling of a somatodendritic cargo protein to an axonally directed kinesin is sufficient to drive transport of whole somatodendritic vesicles through the PAEZ toward the distal axon. Based on these findings, we propose that polarized sorting of transport vesicles occurs at the PAEZ and depends on the ability of the vesicles to acquire an appropriately directed microtubule motor.

INTRODUCTION

Neurons are highly polarized cells featuring distinct somatodendritic and axonal domains (reviewed by [Lasiacka and Winckler, 2011](#)). Biosynthetic sorting of transmembrane proteins to each of these domains occurs by selective incorporation of the proteins into different populations of somatodendritic and axonal carrier vesicles in the neuronal soma ([Fariás et al., 2012](#); [Petersen et al., 2014](#)). These vesicles subsequently move to their corresponding neuronal domains along cytoskeletal tracks (reviewed by [Kapitein and Hoogenraad, 2011](#)). The boundary between the somatodendritic and axonal domains has been located at the axon initial segment (AIS), a specialized region of the proximal axon comprising a high concentration of surface voltage-gated ion channels and cell-adhesion molecules that are anchored by a submembranous assembly of ankyrin G (AnkG) and β IV-spectrin ([Kordeli et al., 1995](#); [Berghs et al., 2000](#); [Ango et al., 2004](#); [Jenkins and Bennett, 2001](#); [Gar-](#)

[rido et al., 2003](#); [Hedstrom et al., 2007](#)). The voltage-gated ion channels perform the main function of the AIS, which is the generation of action potentials in response to somatodendritic inputs. Additionally, the highly ordered structure of the AIS constitutes a barrier for the diffusional mobility of plasma membrane proteins and lipids between the somatodendritic and axonal domains ([Kobayashi et al., 1992](#); [Winckler et al., 1999](#); [Nakada et al., 2003](#)).

The AIS also was proposed to contain a cytoplasmic filter that allows passage of axonal, but not somatodendritic, vesicles toward the distal axon ([Song et al., 2009](#)). This vesicle-sorting function of the AIS was shown to depend on a network of polarized actin filaments that act as a physical barrier for entry of somatodendritic vesicles ([Song et al., 2009](#)) or as tracks for myosin-Va-dependent retrieval of somatodendritic vesicles that enter into the AIS ([Lewis et al., 2009](#); [Watanabe et al., 2012](#); [Al-Bassam et al., 2012](#)). The notion of the AIS as an actin-based filter for segregation of somatodendritic and axonal vesicles, however, has been challenged recently by several findings. First, analysis by platinum replica electron microscopy revealed that the AIS cytoplasm does not contain polarized actin arrays or a dense actin network, but only exhibits sparse actin filaments with mixed orientation ([Jones et al., 2014](#)). Furthermore, although treatment with drugs that disrupt filamentous actin abrogates the polarized distribution of some proteins ([Winckler et al., 1999](#); [Song et al., 2009](#)), this has been shown to result from altered sorting into the corresponding transport vesicles at the soma ([Petersen et al., 2014](#)). Finally, live-cell imaging experiments showed that, during neuronal development in culture, polarized transport of somatodendritic and axonal vesicles is established before the appearance of the AIS ([Petersen et al., 2014](#)). These findings prompted us to reassess the role of the AIS in sorting somatodendritic and axonal vesicles. In particular, we asked where the sorting of somatodendritic and axonal vesicles takes place, and what prevents somatodendritic vesicles from entering the axon.

The results of our study show that sorting of most somatodendritic and axonal carrier vesicles in hippocampal neurons occurs not at the AIS but at a more proximal pre-axonal exclusion zone (PAEZ) located in the axon hillock or at the base of axons that emanate from dendrites. Most somatodendritic vesicles budding from the Golgi complex fail to enter the axon at the PAEZ. This structure excludes not only somatodendritic vesicles but also larger organelles, such as the Golgi complex and the

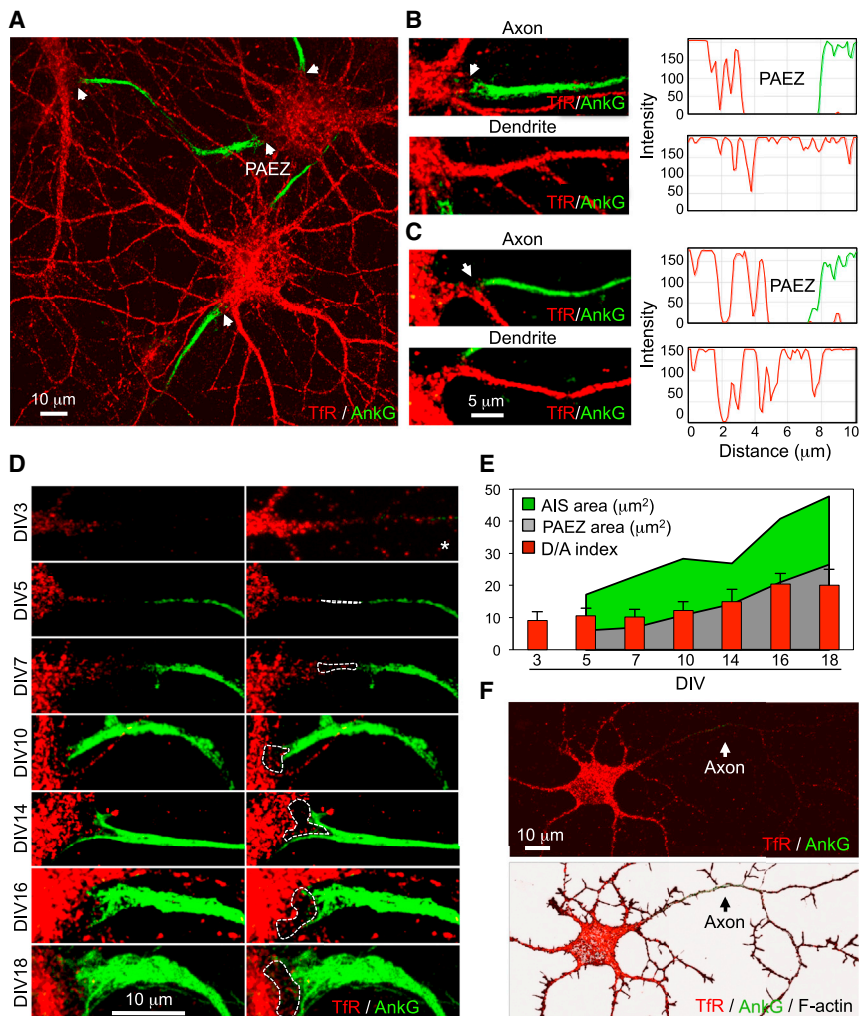


Figure 1. Identification of the PAEZ

(A) The z stack reconstruction of confocal sections from DIV10 hippocampal neurons stained for endogenous TfR (red) and AnkG (green) is shown. (B and C) Magnified views of axons emanating from the soma (B) or from a dendrite (C) and their neighboring dendrites. Graphs on the right show the corresponding TfR and AnkG intensity scans over a 10- μm line running from the soma to the axon or dendrite. In (A)–(C), arrows point to the pre-axonal exclusion zone (PAEZ).

(D) Images of axons emanating from the soma in neurons stained as in (A) at different times in culture. The PAEZ is the area delimited by dashed lines (images on the right). The top right picture marked with an asterisk is a higher intensity image of the top left image.

(E) Graph representing the AIS area (green), PAEZ area (gray), and dendrite/axon (D/A) polarity index (red bars), calculated from 25 neurons at different days of culture in vitro. D/A values are the mean \pm SD.

(F) General view shows the same DIV3 neuron as in the top of (D) co-stained with phalloidin (grayscale, bottom) to highlight F-actin in the entire cytoplasm.

rough ER, in effect constituting the cytoplasmic boundary for the somatodendritic and axonal domains. Fusion of a kinesin light chain (KLC)-binding sequence (KBS) to a somatodendritic protein overcomes exclusion at the PAEZ, promoting transport of whole somatodendritic vesicles through the PAEZ and AIS, all the way to the distal axon. On the basis of these findings, we propose that sorting of somatodendritic and axonal vesicles at the PAEZ depends on the ability of the vesicles to acquire an appropriately directed microtubule motor.

RESULTS

Identification of the PAEZ

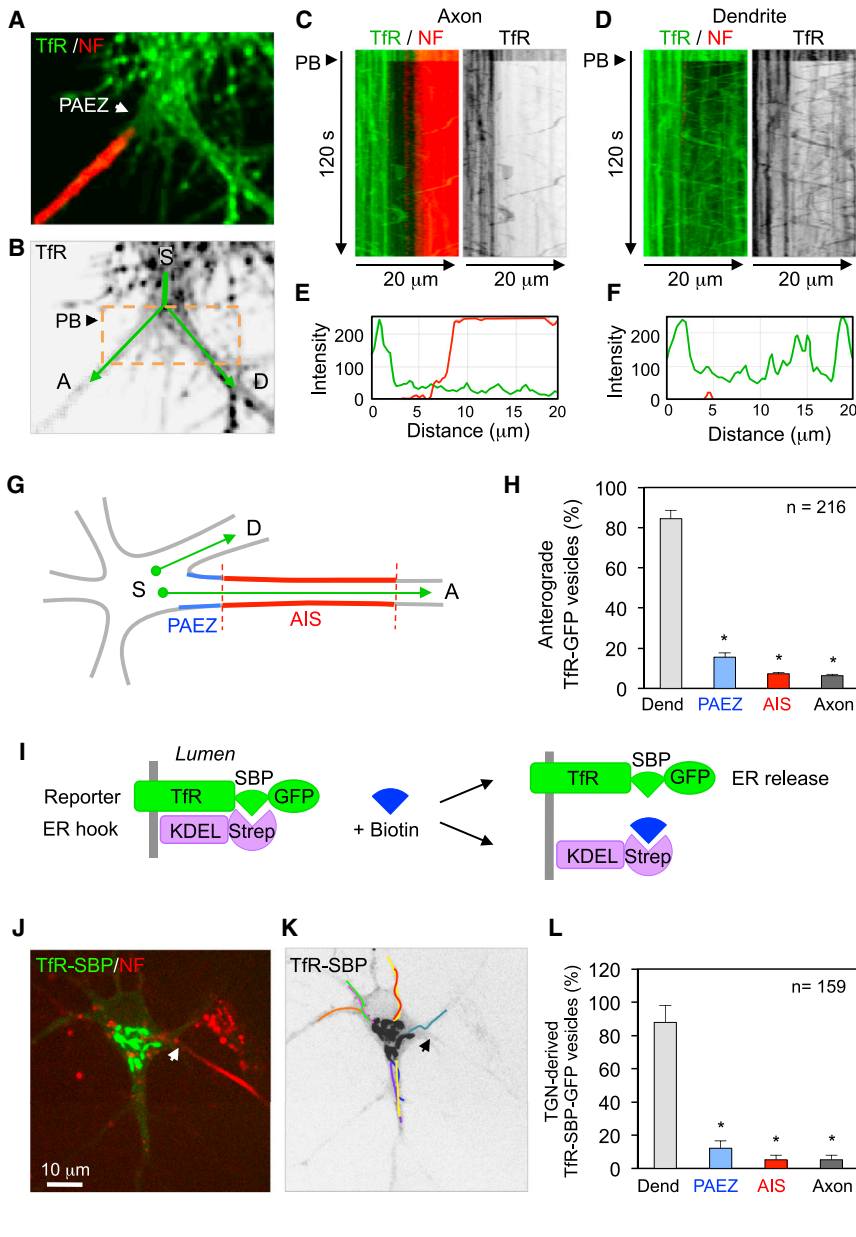
To visualize the cytoplasmic boundary between the somatodendritic and axonal domains, we performed immunofluorescent staining of the endogenous transferrin receptor (TfR) (a somatodendritic protein) (Cameron et al., 1991) and AnkG (an AIS marker) (Kordeli et al., 1995) in 10-day-in-vitro (DIV10) cultured rat hippocampal neurons (Dotti et al., 1988; Kaech and Banker, 2006), followed by optical sectioning and z stack reconstruction on a confocal microscope. This analysis re-

vealed a region of the cytoplasm devoid of fluorescence between the soma and the proximal edge of the AIS (Figure 1A, arrowheads). This clear region occurred within the axon hillock (Figure 1B) or at the base of axons emanating from dendrites (Figure 1C). In contrast, the transition zone from the soma to the dendrites exhibited a continuous distribution of TfR (Figures 1B and 1C). The clear region thus represented a subdomain of the neuronal cytoplasm proximal to the AIS

from which TfR-containing vesicles were excluded and is the region we named the PAEZ. During neuronal development in culture, the AIS (as visualized by AnkG staining) first appeared at DIV4 or DIV5 and, subsequently, grew in size until the final point of our experiment (DIV18) (Figures 1D and 1E). The PAEZ already was apparent at DIV5 and became progressively larger until DIV18 (Figures 1D and 1E). Importantly, the endogenous TfR exhibited somatodendritic polarity (dendrite/axon polarity index \sim 9) from DIV3, before assembly of the AIS (Figures 1D and 1F), in agreement with previous work using TfR-GFP expressed by transient transfection (Petersen et al., 2014). Thus, exclusion of the TfR occurs at a region that precedes, both spatially and temporally, the AIS.

Somatodendritic Vesicles Are Excluded from the Axon at the PAEZ

To examine the dynamic behavior of TfR-containing vesicles in relation to the PAEZ and AIS, we performed live-cell imaging of DIV10 neurons expressing GFP-tagged TfR (TfR-GFP) that were surface labeled with a CF555-conjugated antibody to the AIS adhesion protein neurofascin (NF) (Ango et al., 2004;



Hedstrom et al., 2007; [Movie S1](#); [Figure 2A](#)). Photobleaching (PB) of an area around the PAEZ was performed to facilitate visualization of vesicle movement over a dark background ([Figure 2B](#)). Time-lapse imaging ([Movie S1](#)) and kymographs ([Figures 2C–2F](#)) showed that most TFR-GFP-containing vesicles were unable to enter the PAEZ (dark band between green and red in [Figure 2C](#)), in contrast to their unimpeded movement into a comparable region of a neighboring dendrite over a 120-s time span. Quantification of results from 15 neurons showed that, of all the TFR-GFP vesicles proceeding from an area of the soma ([Figure 2G](#)), only 15.5% entered the PAEZ while 84.5% entered the neighboring dendrite ([Figure 2H](#)). Of those vesicles that penetrated the PAEZ, about half returned to the soma from within the PAEZ, while the other half reached the

AIS and then either turned back or proceeded toward the distal axon ([Figure 2H](#)). These observations indicated that axonal exclusion of most anterograde, TFR-GFP-containing vesicles occurred at the PAEZ.

Because between one-third and two-thirds of TFR-GFP-containing vesicles observed under these conditions are endosomes ([Petersen et al., 2014](#)), we sought to limit our analysis to somatodendritic vesicles carrying newly synthesized TFR-GFP that emanated from the Golgi complex. To this end, we used the RUSH system ([Boncompain et al., 2012](#)), a recently developed procedure that allows retention of proteins in the ER followed by their synchronous release and transport through the secretory pathway ([Figure 2I](#)). We observed that, 20 min after release from the ER in DIV7 neurons, most TFR-GFP became

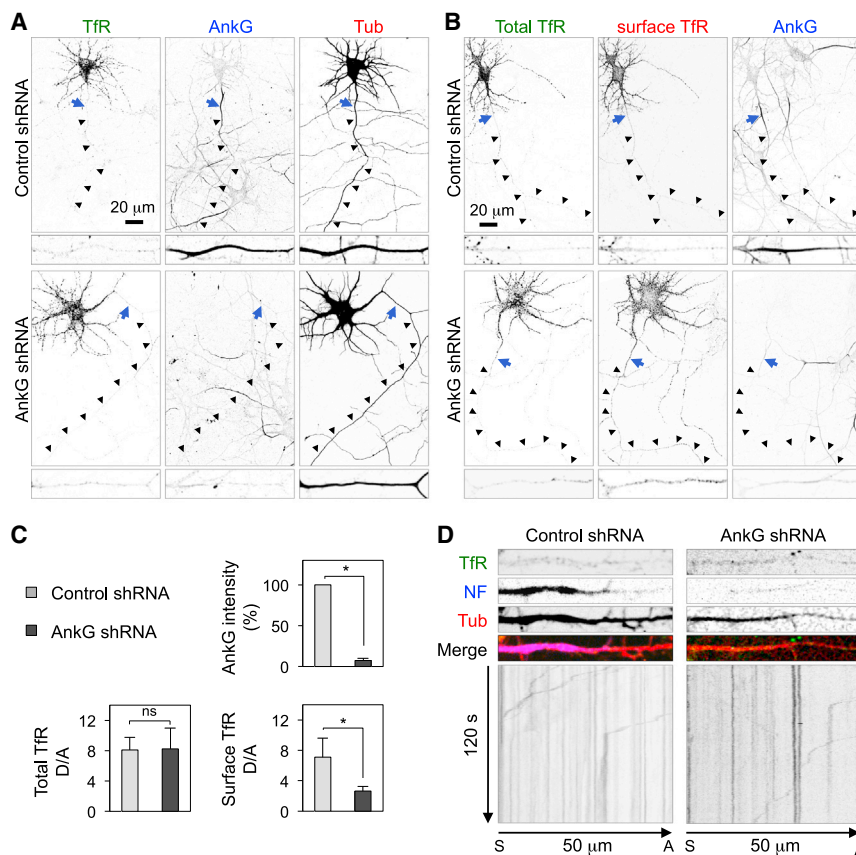


Figure 3. Axonal Exclusion of Somatodendritic Vesicles in the Absence of the AIS

(A) DIV3 neurons were co-transfected with plasmids encoding control shRNA or AnkG shRNA, together with TfR-GFP and mCherry-tubulin, and stained for AnkG on DIV8.

(B) DIV3 neurons co-transfected with plasmids encoding control shRNA or AnkG shRNA, together with TfR-GFP, were surface stained live with CF555-conjugated antibody to GFP prior to fixation and staining for AnkG on DIV8. Enlarged regions of axon are shown at the bottom of each image. Arrows indicate the position of the AIS and arrowheads trace the trajectory of the axon.

(C) Graph represents AnkG intensity (%) and dendrite/axon (D/A) ratio for total and surface TfR-GFP quantified from 20 neurons and expressed as mean \pm SD (* $p < 0.001$; ns, not significant).

(D) Images of axons from live DIV8 neurons transfected as in (A) and stained for NF. Grayscale kymographs for TfR-GFP recorded every 500 ms for 120 s were generated from a straightened 30-pixel-wide line along a 50- μ m path of an axon. Particles moving in retrograde direction appear as lines with positive slopes. See also [Movie S3](#).

The PAEZ Is a Boundary for the Distribution of Various Cytoplasmic Organelles

Staining for TfR-GFP of control neurons at the cell surface showed that this protein was not excluded from the plasma

membrane but only from the cytoplasm of the PAEZ ([Figure S1](#)). To further characterize the properties of the PAEZ in comparison to the AIS, we examined the distribution of other organelle markers. Staining for AnkG was largely coincident with that for other AIS components, including NF, β IV-spectrin, and voltage-gated sodium channels detected with the PanNav antibody ([Figure 4A](#)). None of these proteins were present in significant amounts at the PAEZ, demonstrating that this structure is physically distinct from the AIS. Several other markers were excluded from both the PAEZ and AIS, including the somatodendritic AMPA-type glutamate receptor GluR1, the Golgi matrix protein GM130, the *trans*-Golgi network (TGN) protein TGN38, and the CLIMP-63 protein, which links the rough ER to microtubules ([Figure 4A](#)). In contrast, structures staining for the smooth ER protein reticulon (RTN), the mitochondrial dye MitoTracker (Mito), the lysosomal dye LysoTracker (Lyso), and the axonal cell-adhesion molecule NgCAM/L1 penetrated the PAEZ and AIS all the way toward the distal axon ([Figure 4A](#)). These observations indicated that the differential distribution of various cytoplasmic organelles between the somatodendritic and axonal domains ([Raine, 1999](#)) is established at the level of the PAEZ. The clathrin-associated AP-1 complex involved in cargo sorting into somatodendritic vesicles ([Dwyer et al., 2001](#); [Margeta et al., 2009](#); [Farias et al., 2012](#); [Mattera et al., 2014](#); [Jain et al., 2015](#)) also was excluded at the PAEZ, but the homologous AP-2 complex involved in endocytosis at both pre- and post-synaptic sites ([Maycox et al., 1992](#);

concentrated in the Golgi area ([Figure 2J](#); [Movie S2](#)). Subsequent live-cell imaging over a 120-s period revealed that most vesicles budding from the Golgi entered an average dendrite, but not the PAEZ ([Figures 2K and 2L](#); [Movie S2](#)). Thus, bona fide somatodendritic carrier vesicles budding from the Golgi also were prevented from entering the axon at the PAEZ.

Axonal Exclusion of Somatodendritic Vesicles Occurs Independently of the AIS

To analyze further if the presence of the AIS was necessary for exclusion of somatodendritic vesicles from the axon, we prevented assembly of the AIS by treatment of DIV3 neurons with a small hairpin RNA (shRNA) to AnkG ([Hedstrom et al., 2008](#)), and we examined the distribution of TfR-GFP and the movement of TfR-GFP-containing vesicles at DIV8. We observed that this treatment precluded the appearance of AnkG, but did not alter the overall somatodendritic polarity of TfR-GFP in fixed-permeabilized neurons ([Figures 3A and 3C](#)). Staining of live neurons, however, revealed an increase in surface TfR-GFP in the axon of AnkG-depleted neurons relative to control neurons ([Figures 3B and 3C](#)). Nevertheless, live-cell imaging showed that most TfR-GFP-containing vesicles remained unable to enter the axon in the absence of the AIS ([Figure 3D](#); [Movie S3](#)). From these experiments, we concluded that blocking formation of the AIS at early stages of neuronal development did not abolish the ability of neurons to exclude most TfR-GFP-containing carriers from the axon.

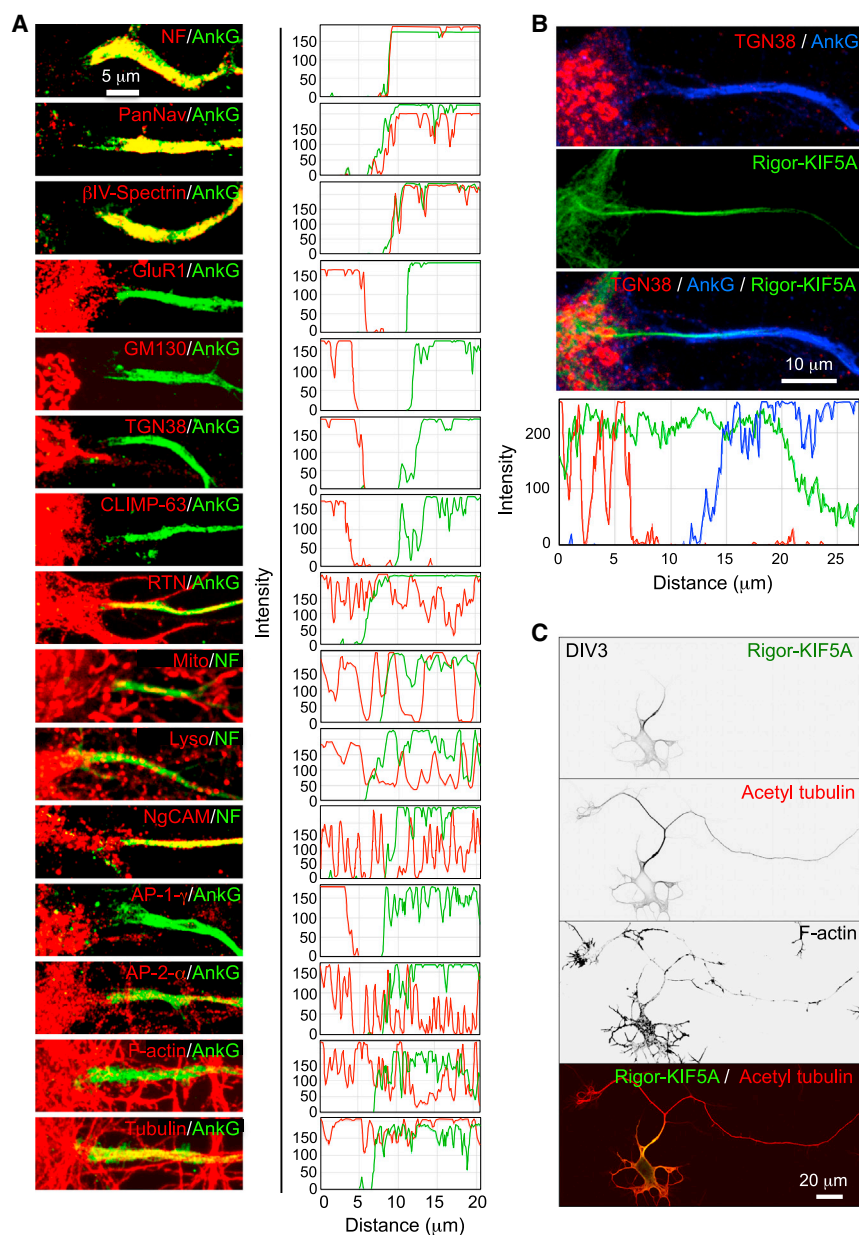


Figure 4. Selective Exclusion of Somatodendritic Organelles and Presence of KIF5 Microtubule Tracks in the PAEZ

(A) (Left) Images of the soma-PAEZ-AIS transitional region from DIV10 neurons stained for AIS markers (AnkG or NF) and the indicated organellar markers (see Results for description of these markers). (Right) Corresponding fluorescence line intensity scans are shown.

(B) DIV10 neurons expressing GFP-Rigor-KIF5A (green), co-stained for AnkG (blue) and TGN38 (red), and corresponding line intensity scans are shown.

(C) DIV3 neurons expressing GFP-Rigor-KIF5A (green), co-stained for acetylated α -tubulin (red) and F-actin (grayscale), are shown.

anterograde transport of organelles such as axonal carrier vesicles (Kamal et al., 2000; Song et al., 2009) and mitochondria (Hurd and Saxton, 1996) along the axon occurs through association with the plus-end-directed microtubule motor KIF5 (i.e., also known as kinesin heavy chain or kinesin-1) (Vale et al., 1985; Brady, 1985; Aizawa et al., 1992). The initial site of recruitment of KIF5 to axonal microtubules can be highlighted by expression of a rigor KIF5 mutant that binds to microtubules, but cannot walk along them (Nakata and Hirokawa, 2003). We observed that a Rigor-KIF5A (neuron-specific A isoform of KIF5) construct decorated a track that spanned the PAEZ (Figure 4B). This track could be visualized as early as DIV3, simultaneously with the appearance of tubulin modifications typical of axonal microtubules (e.g., acetylation) (Reed et al., 2006; Hammond et al., 2010; Figure 4C) and prior to the assembly of the AIS (Figures 1D–1F and S3).

The above considerations led us to hypothesize that somatodendritic vesicles might be excluded from the PAEZ

(Lavezzari et al., 2003) was not excluded (Figure 4A). Filamentous actin was present, but not particularly concentrated, at the PAEZ and AIS (Figures 4A and S2), in line with recent observations (Jones et al., 2014). Tubulin, on the other hand, was abundant at the PAEZ (Figure 4A), consistent with the origin of axonal microtubules in this region of the neuron (Palay et al., 1968; Braun et al., 1993).

Binding to Kinesin-1 Missorts Somatodendritic Proteins to the Axon

We next addressed the question of what keeps somatodendritic vesicles from entering the PAEZ. In general, particles larger than 260 Å in radius are unable to diffuse in the cytoplasm (Luby-Phelps et al., 1987), unless driven by molecular motors. Indeed,

because they fail to bind an axonal kinesin such as KIF5. In most cases, KIF5 functions as part of an oligomeric complex comprising two KIF5 and two KLC subunits (Vale et al., 1985; Brady, 1985; Hirokawa et al., 1989; DeBoer et al., 2008). KLC contains an amino-terminal heptad repeat domain that binds to KIF5 and a carboxy-terminal tetratricopeptide repeat (TPR) domain that participates in cargo recognition (Gauger and Goldstein, 1993; Gindhart and Goldstein, 1996). To test if conferring binding to KIF5 could overcome the exclusion of somatodendritic vesicles at the PAEZ, we fused three copies of the KBS TNLEWDDSAI from the cargo adaptor protein SKIP (Pernigo et al., 2013; Pu et al., 2015) to the cytosolic tails of two somatodendritic cargo proteins, TfR and Nipah Virus F glycoprotein (NiV-F) (Mattera et al., 2014; Figure 5A). We observed that fusion

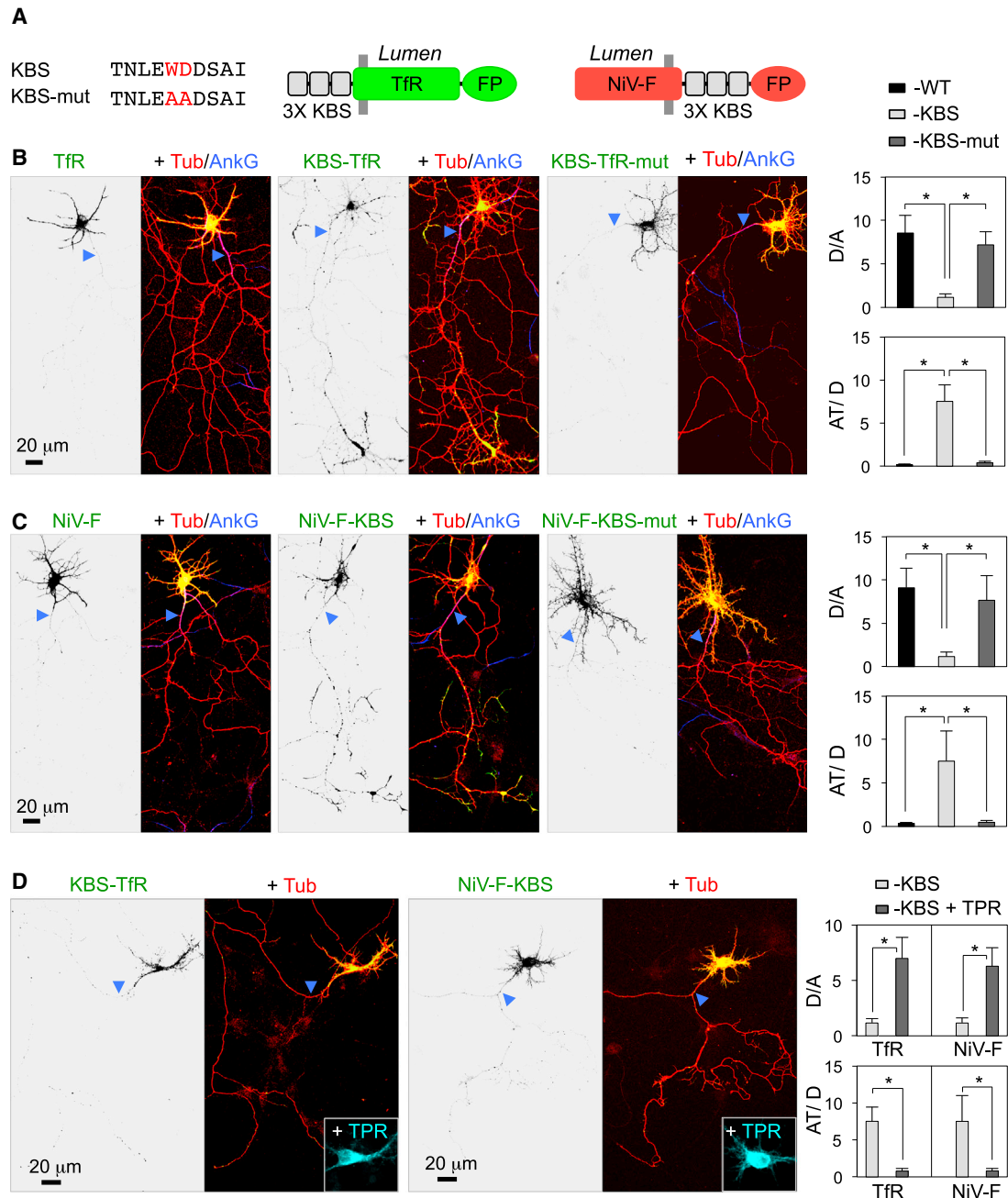


Figure 5. Fusion of a KLC-Binding Sequence to Somatodendritic Proteins Causes Missorting of the Chimeras to the Axon

(A) Three copies of the KLC-binding sequence (KBS) from SKIP (Pernigo et al., 2013) or an inactive WD-to-AA mutant of it (KBS-mut) were fused to the cytosolic N terminus of TfR or C terminus of NiV-F, both tagged with fluorescent proteins (FPs, GFP or mCherry).

(B and C) DIV7 neurons co-expressing mCherry-tubulin (Tub, red) with TfR-GFP (B) or NiV-F-GFP (C), wild-type (WT, left) or fused to KBS (middle) or KBS-mut (right), were immunostained for AnkG (blue). Enlarged regions of the somatodendritic domain and axon tips are shown in Figure S4. Dendrite/axon (D/A) and axon tip/dendrite (AT/D) ratios were quantified from 25 neurons and expressed as mean \pm SD ($*p < 0.001$).

(D) DIV7 neurons co-expressing KBS-TfR-GFP (left) or NiV-F-KBS-GFP (right), mCherry-tubulin (Tub, red), and the dominant-negative KLC TPR-HA (cyan). D/A and AT/D ratios were quantified from 25 neurons and expressed as mean \pm SD ($*p < 0.001$). In all images, arrowheads point to the AIS.

of the triple KBS, but not an inactive mutant having a substitution of WD to AA (Pernigo et al., 2013), redirected both cargo proteins from the somatodendritic domain to axons, particularly axon tips (Figures 5B, 5C, and S4). Fusion of one or two copies of the KBS

had a similar effect, although with less concentration at axon tips (Figure S5). Axonal mistargeting of KBS-TfR and NiV-F-KBS was prevented by co-expression of a dominant-negative KLC construct comprising only the KBS-binding TPR domain (Verhey

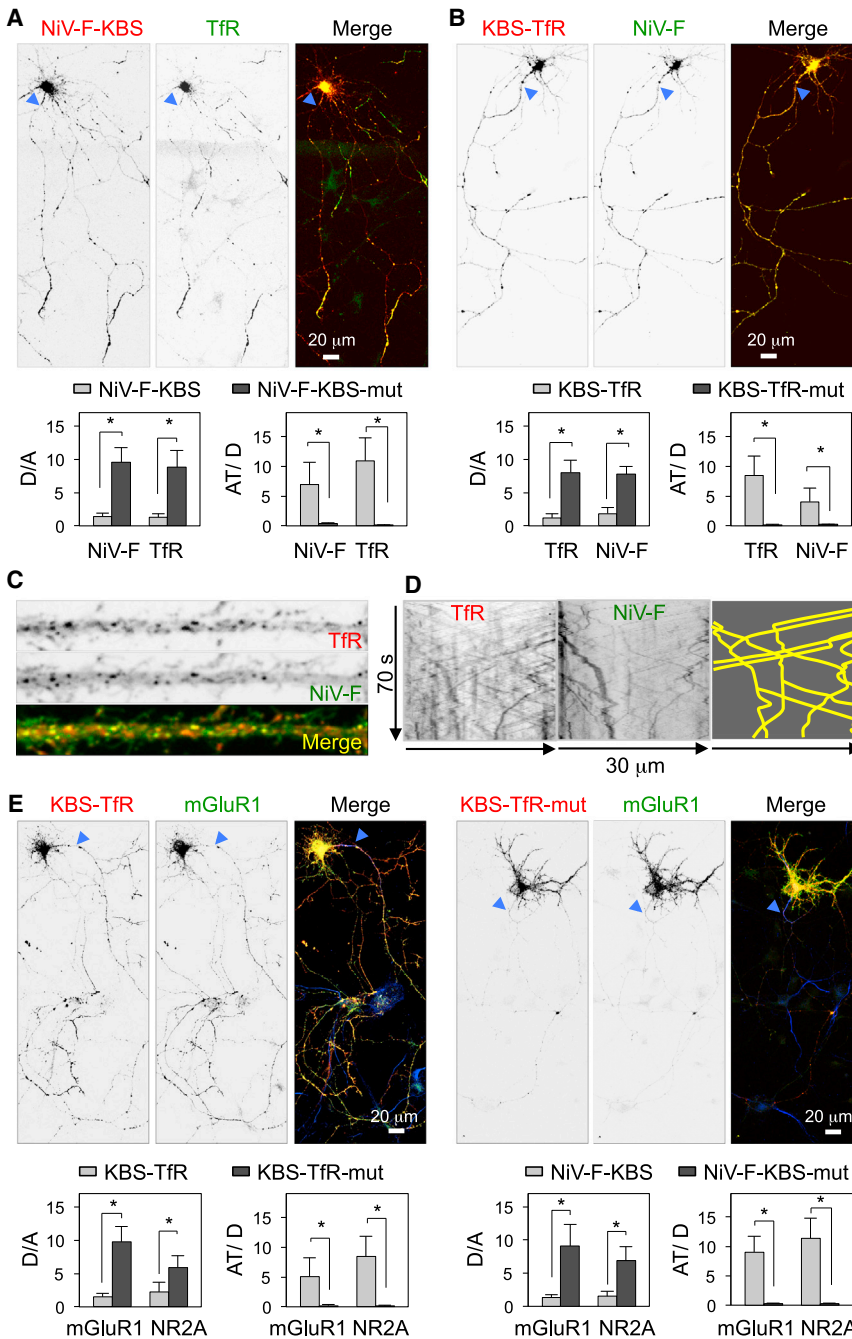


Figure 6. NiV-F-KBS and KBS-TfR Chimeras Redirect Other Somatodendritic Proteins to the Axon

(A) Expression of NiV-F-KBS-mCherry (red) redirects TfR-GFP (green) to the axon in DIV7 neurons. NiV-F-KBS-mCherry also redirects endogenous TfR to the axon (Figure S7). D/A and AT/D ratios of WT NiV-F and TfR proteins in neurons expressing NiV-F-KBS-mCherry, or the corresponding NiV-F-KBS-mut constructs, are shown.

(B) Expression of KBS-TfR-mCherry (red) redirects NiV-F-GFP (green) to the axon in DIV7 neurons. D/A and AT/D ratios of TfR and NiV-F proteins in neurons expressing KBS-TfR-mCherry, or the corresponding KBS-TfR-mut constructs, are shown.

(C) Dendrite from a DIV10 neuron shows co-localization of TfR-mCherry (red) and NiV-F-GFP (green) to the same vesicles.

(D) Grayscale kymographs for TfR-mCherry (left) and NiV-F-GFP (middle) corresponding to a DIV10 neuron recorded every 500 ms for 70 s were generated from a straightened 20-pixel-wide line along a 30- μ m path of a dendrite. Co-movement of particles is indicated as yellow tracks (right).

(E) DIV7 neurons co-transfected with plasmids encoding mGluR1-GFP (grayscale in the middle and green in the right merged images) plus KBS-TfR-mCherry or KBS-TfR-mut-mCherry (grayscale in the left and red in the right merged images). Notice the redistribution of mGluR1-GFP to axons and axon tips upon KBS-TfR-mCherry, but not KBS-TfR-mut, expression. D/A and AT/D ratios of mGluR1-GFP and NR2A-GFP proteins in neurons expressing KBS-TfR-mCherry, NiV-F-KBS-mCherry, or the corresponding KBS-mut constructs are shown. In all images, arrowheads point to the AIS. In all graphs, the values are the mean \pm SD from 25 neurons ($*p < 0.001$).

of KIF13A (Huang and Banker, 2012) fused to streptavidin (Figure S6).

Redirection of Whole Somatodendritic Vesicles to the Axon by Binding to Kinesin-1

To determine whether fusion of the triple KBS to a particular somatodendritic protein affected the polarity of other somatodendritic proteins, we examined the effect

of expressing NiV-F-KBS on the distribution of co-expressed TfR-GFP (Figure 6A) and endogenous TfR (Figure S7). Indeed, we observed that expression of NiV-F-KBS caused missorting of both TfR forms to the axon, even though the latter proteins lacked the KBS. Similarly, expression of KBS-TfR missorted NiV-F-GFP to the axon (Figure 6B). These observations were consistent with the fact that NiV-F and TfR are transported in the same somatodendritic vesicles (Figures 6C and 6D). Moreover, we found that expression of KBS-TfR or NiV-F-KBS also caused axonal missorting of the glutamate receptor proteins

(et al., 2001; Figure 5D). Expression of this construct not only precluded axonal localization of KBS-TfR and NiV-F-KBS but also restored their localization to dendrites (Figure 5D). These observations thus demonstrated that axonal mistargeting of KBS-TfR and NiV-F-KBS was mediated by interaction with kinesin-1, while also showing that dendritic localization of these cargos was independent of this kinesin. Axonal mistargeting of TfR and NiV-F appended with a streptavidin-binding peptide (SBP) also was achieved by co-expression of these proteins with a chimeric protein comprising the axonally directed motor domain

mGluR1 and NR2A (Figure 6E), indicating that all of these proteins are transported in the same somatodendritic vesicles. These experiments thus demonstrated that endowing a somatodendritic cargo with the ability to bind kinesin-1 is sufficient to redirect whole somatodendritic vesicles, with their full complement of cargos, to the axon.

Tubulin Acetylation Controls the Ability of Kinesin-1 to Redirect Somatodendritic Cargos to the Axon

The preference of kinesin-1 for axonal microtubules is likely specified by combinations of post-translational modifications of tubulin subunits, including acetylation of α -tubulin at lysine-40 (Reed et al., 2006; Hammond et al., 2010). To determine if this latter modification influenced the ability of kinesin-1 to direct KBS-TfR and NiV-F-KBS to the axon, we examined the effects of overexpressing the acetylation mimic K40Q mutant of α -tubulin. We observed that overexpression of this mutant abrogated the preferential association of Rigor-KIF5A with axonal microtubules (Figure 7A) and reduced the axonal missorting of KBS-TfR and NiV-F-KBS (Figures 7B and 7C). Therefore, tubulin acetylation contributes to the specificity of kinesin-1 for cargo transport to the axon.

DISCUSSION

Our findings lead us to conclude that sorting of somatodendritic and axonal vesicles occurs at the PAEZ rather than the AIS (Figure 7D). It is well established that the AIS functions as a barrier for lateral diffusion of proteins and lipids at the plasma membrane (Winckler et al., 1999; Kobayashi et al., 1992; Nakada et al., 2003). In addition, long-term ablation of the AIS in rat hippocampal neurons by treatment with AnkG shRNA from DIV10 to DIV20 (Hedstrom et al., 2008) or in Purkinje neurons by a cerebellum-specific mutation of the AnkG gene in mice (Sobotzik et al., 2009) causes redistribution of somatodendritic proteins to the axon. However, studies of cortical neuron development in mouse embryos showed that initial axon specification and establishment of axonal-dendritic polarity occur independently of AnkG and the AIS (Galiano et al., 2012). These latter findings are consistent with our observations that TfR already exhibits somatodendritic polarity at DIV3 in cultured rat hippocampal neurons, well before assembly of the AIS (Figures 1D–1F). Moreover, prevention of AIS assembly between DIV3 and DIV8 by AnkG shRNA treatment does not abolish overall TfR somatodendritic polarity and exclusion of most TfR-containing vesicles from the axon, although some TfR begins to appear on the axonal surface (Figure 3). Taken together, these data suggest two phases in the mechanisms of neuronal polarity: an early establishment phase that is independent of AnkG and the AIS, and a later maintenance phase that requires AnkG and the AIS.

Previous studies showed that somatodendritic vesicles either stopped at the proximal edge of the AIS (Petersen et al., 2014) or entered the AIS but were retrieved by Myosin-Va-dependent transport (Lewis et al., 2009; Watanabe et al., 2012). At variance with these studies, we find that most somatodendritic vesicles fail to enter the axon at a more proximal region in the axon hillock or the base of axons that emanate from dendrites, which we define as the PAEZ. Several differences in experimental design

could account for these discordant results. First, our initial visualization of the PAEZ was enabled by immunofluorescent staining of endogenous somatodendritic (TfR) and AIS (AnkG) markers, followed by optical sectioning and z stack reconstruction on a confocal microscope (Figures 1A–1D). Second, in our live-cell experiments, transgenic TfR-GFP and endogenous NF were always imaged simultaneously (Figure 2), so that the position and trajectory of somatodendritic vesicles relative to the PAEZ and AIS could be determined unambiguously. Finally, and perhaps most importantly, we tracked somatodendritic vesicle movement toward the axon and an adjacent dendrite from a region deeper in the perikaryal cytoplasm (Figure 2G). This revealed a substantial difference in the number of somatodendritic vesicles entering the PAEZ (12.1%–15.5%) relative to those entering an adjacent dendrite (84.5%–87.9%) (Figures 2H and 2L). In previous studies, the starting region for imaging of somatodendritic vesicles may have included the PAEZ, in which case the behavior of the observed vesicles would correspond to that of the smaller fraction that had already entered this zone.

The PAEZ described here is likely a cytoplasmic region devoid of Nissl bodies or tigroid substance in the axon hillock that was observed by cytochemical staining as early as the 19th century (e.g., Figures 1 and 2 in the article by Held, 1895; see also Braun et al., 1993). The Nissl dye stains a basophilic substance that mostly corresponds to RNA of polyribosomes associated with the rough ER (Palay and Palade, 1955). This substance is found throughout the soma and dendrites, but is absent from the axon hillock and axon (Braun et al., 1993). A similar pattern was observed by labeling of the Golgi complex with the lectin wheat germ agglutinin (WGA) (Braun et al., 1993). For both Nissl and WGA staining, an abrupt transition in the cytoplasm was evident between the perikaryon and the axon hillock (Braun et al., 1993). Electron microscopy studies confirmed the absence of rough ER and Golgi complex in the axon hillock, but showed the presence of other organelles, such as smooth ER, mitochondria, multivesicular bodies (i.e., late endosomes), and various vesicles (Palay et al., 1968; Braun et al., 1993). The axon hillock also was shown to be rich in cytoskeletal elements such as dense microtubule fascicles that funnel into the axon, as well as neurofilaments (Palay et al., 1968; Braun et al., 1993). Beyond the apex of the axon hillock, the plasma membrane acquired an electron-dense undercoating (Palay et al., 1968; Braun et al., 1993) that is now known to correspond to the submembranous ankyrin-G- β IV-spectrin scaffold of the AIS (Kordeli et al., 1995; Berghs et al., 2000). The organelle composition of the axon hillock characterized in these earlier studies is clearly similar to that of the PAEZ defined here (Figure 4). We surmise that the proximal region of axons that arise from dendrites has a similar composition, since it also exhibits properties of the PAEZ (Figures 1A–1C). The exclusion of the rough ER and Golgi complex, in addition to somatodendritic vesicles, at the PAEZ suggests that a common restriction mechanism may operate for all of these organelles.

We were initially interested in further exploring how an actin-based filter could segregate somatodendritic and axonal vesicles. However, confocal fluorescence microscopy of phalloidin-stained neurons did not show any dense F-actin cytoplasmic structure in the AIS or PAEZ (Figures 4A and S2). Higher resolution analyses by other researchers revealed periodic ring-like

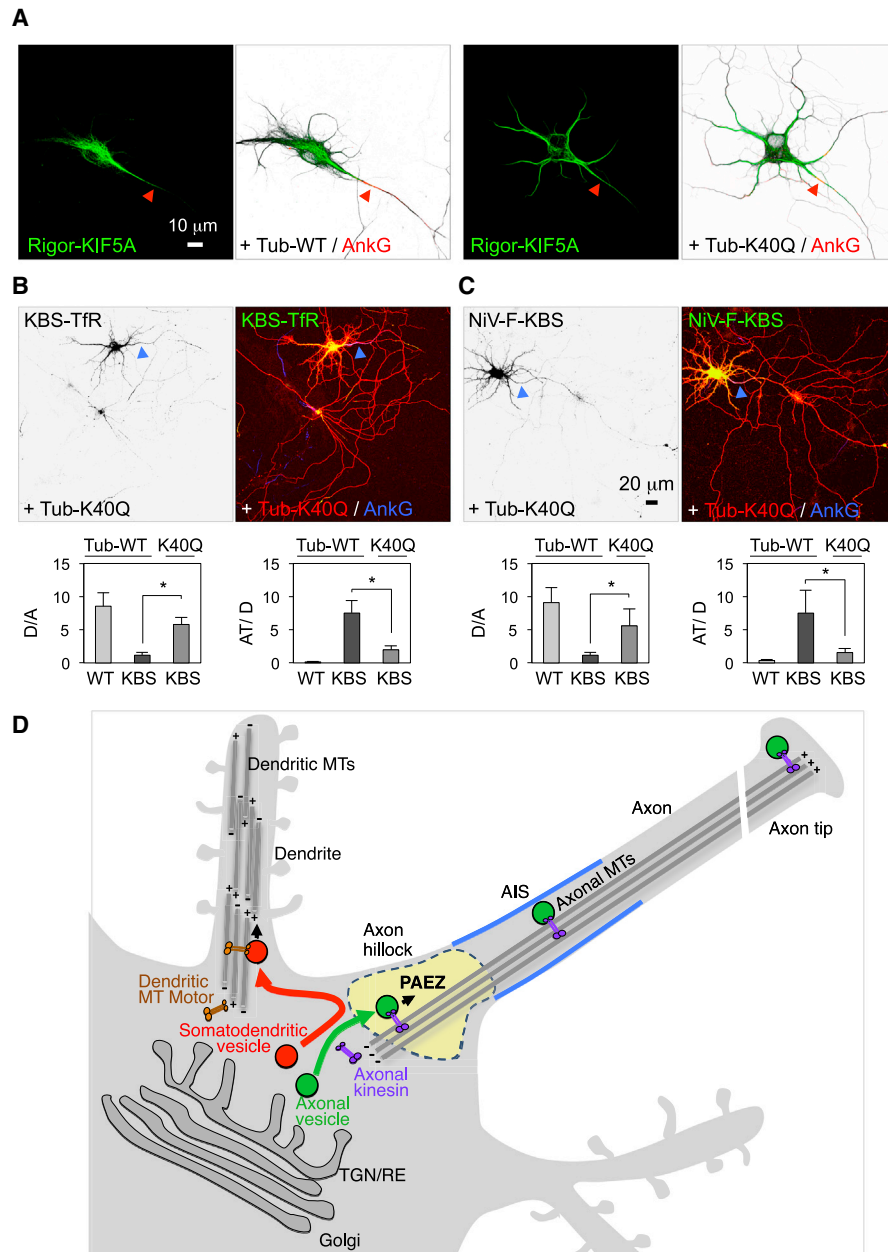


Figure 7. Importance of Tubulin Acetylation and Model for Vesicle Sorting at the PAEZ

(A) DIV7 neurons co-expressing GFP-Rigor-KIF5A (green) with mCherry-tubulin (Tub-WT) (left) or acetylation mimic K40Q mutant α -tubulin (Tub-K40Q) (right). Notice that Tub-K40Q overexpression causes mislocalization of Rigor-KIF5A to dendrites. Arrowheads point to the AIS stained for AnkG (red).

(B and C) Expression of mCh-Tub-K40Q (red) reduces axonal missorting of TfR-KBS-GFP (B, left, green on right side) and NiV-F-KBS-GFP (C, left, green on right side) in DIV7 neurons immunostained for AnkG (blue). D/A and AT/D ratios were quantified from 25 neurons and expressed as mean \pm SD (* $p < 0.001$).

(D) Schematic representation of vesicle sorting at the PAEZ. We propose that polarized sorting of transport vesicles begins at the PAEZ and depends on the ability of vesicles to acquire an axonally directed microtubule motor. Sorting of newly synthesized proteins to the axonal or somatodendritic domains of neurons involves selective incorporation into distinct populations of vesicular transport carriers budding from the *trans*-Golgi network (TGN) or recycling endosomes (REs) (Farias et al., 2012; Petersen et al., 2014). Axonal vesicles associate to axonally directed microtubule (MT) motors such as kinesin-1 at the level of the PAEZ, resulting in movement of the vesicles toward the MT plus end in the distal axon. Somatodendritic vesicles, on the other hand, fail to enter the axon at the PAEZ because they lack the ability to bind axonal MT motors. Instead, these vesicles are driven to dendrites by association with other kinesins or dynein, which mediates transport along the mixed-polarity MTs present in the dendrites.

structures containing actin, spectrin, and associated proteins under the axonal plasma membrane starting at the axon hillock (Xu et al., 2013), but no dense actin meshwork or polarized actin filaments in the cytoplasm of the AIS (Jones et al., 2014). These observations prompted us to seek alternative explanations for the mechanism of vesicle sorting at the PAEZ. We went back to an early notion that only vesicles that bind a specific microtubule motor might be able to enter the axon, while all others remain in the somatodendritic domain (Palay et al., 1968). Indeed, we found that appending a somatodendritic protein with a short peptide sequence (KBS) that binds to kinesin-1 (Perinigo et al., 2013) enabled passage of whole somatodendritic vesicles through the PAEZ and AIS toward the distal axon (Figures 5 and 6). Kinesin-1 is the best known among several plus-end-directed kinesins that mediate preferential transport of carrier vesicles to the axon (Ferreira et al., 1993; Kamal et al., 2000; Song et al., 2009; Huang and Banker, 2012).

The role of kinesin-1 in axonal transport may derive from its selective recruitment to microtubules having specific combinations of post-translational modifications of tubulin (Liao and Gundersen, 1998; Reed et al., 2006; Nakata et al., 2011) that are enriched in the axon beginning at the PAEZ. Indeed, we found that overexpression of an acetylation mimic α -tubulin mutant randomized the distribution of KIF5A to the axon and dendrites and reduced the axonal missorting of KBS-tagged somatodendritic cargos (Figures 7A–7C). Expression of a dominant-negative KLC mutant comprising only the cargo-recognition TPR domain abrogated the axonal, but not dendritic, transport of KBS-tagged somatodendritic proteins (Figure 5D). These findings imply that vesicles carrying the somatodendritic proteins examined in this study (TfR and Niv-F) do not depend on kinesin-1 for transport to the dendrites. Instead, these vesicles might acquire other plus-end-directed kinesins (Setou et al., 2000; Chu et al., 2006; Song et al., 2009; Jenkins et al., 2012; Huang and Banker, 2012) or the minus-end-directed dynein (Zheng et al., 2008; Kapitein et al., 2010) for movement within the somatodendritic domain. The potential use of both plus-end- and minus-end-directed microtubule motors for somatodendritic transport is supported by the existence of mixed-polarity microtubules in the dendrites of hippocampal neurons (Baas et al., 1988; Burton, 1988). Exactly which among the ~45 mammalian kinesins could mediate axonal versus somatodendritic transport is currently a matter of debate, because the direction of transport may be influenced by interactions with specific cargos (Atherton et al., 2013). Finally, the actin motor myosin Va also could play a role in directing vesicles to the dendrites (Lewis et al., 2009), as it does in transport from the dendritic shaft to spines (Correia et al., 2008).

Our results are, thus, most consistent with a model in which polarized sorting of carrier vesicles (and likely other cytoplasmic organelles) at the PAEZ is microtubule based and dependent on the differential acquisition of microtubule motors that mediate selective transport to the axon or dendrites (Figure 7D). Organelles that normally bind kinesin-1 or other axonal kinesins can traverse the PAEZ en route to the distal axon, while those that do not bind axonal kinesins cannot pass through the PAEZ and instead are directed to the dendrites by other kinesins or dynein.

EXPERIMENTAL PROCEDURES

Cell Culture and Transfection

Primary hippocampal neuronal cultures were prepared as previously described (Kaech and Banker, 2006). Briefly, hippocampi were dissected from Sprague-Dawley rats on embryonic day 18. Cells were dissociated and plated onto poly-L-lysine-treated plates and maintained in DMEM supplemented with 10% horse serum for ~3 hr at 37°C under a humidified atmosphere (95:5, air:CO₂). The culture medium was substituted with Neurobasal medium supplemented with B-27 and Glutamax. After 4–6 days in culture, neurons were transfected with different constructs using Lipofectamine 2000, except for the localization of GFP-Rigor-KIF5A on DIV3 when transfection was performed on DIV2. NgCAM, smooth ER, and rough ER were detected by transfection with plasmids encoding NgCAM (0.2 μ g), GFP-RTN (25 ng), and RFP-CLIMP-63 (25 ng), respectively, and immunostaining with monoclonal anti-NgCAM or polyclonal anti-GFP that recognizes both GFP and RFP. Transfected and untransfected neurons were analyzed after different days in culture, as indicated in the figure legends. The AIS was identified by immunostaining with antibody to AnkG for fixed neurons or CF488-, CF555-, or CF640-conjugated antibody to NF for live neurons.

Immunofluorescence and Confocal Microscopy

Neurons were fixed with 4% paraformaldehyde and 4% sucrose in PBS for 20 min, permeabilized with 0.2% Triton X-100 for 15 min, blocked with 0.2% porcine gelatin for 30 min at 37°C, and stained with primary antibodies for 30 min at 37°C, followed by secondary antibodies for 30 min at 37°C. For TfR-GFP surface staining, we incubated live neurons with CF555-conjugated antibody to GFP for 30 min at 4°C. Cells were then fixed, permeabilized, and stained with antibody to AnkG, followed by appropriate secondary antibodies. All fluorescence images were obtained using a confocal microscope (LSM710, Zeiss) equipped with 63 \times 1.4 numerical aperture (NA) and 40 \times 1.3 NA objectives. A small pinhole and z stacks were used to characterize the PAEZ. The z stack reconstructions were performed using ImageJ version 1.44o (Wayne Rasband, NIH, <http://imagej.nih.gov>). All image analysis, including fluorescence line intensity plots and calculation of dendrite/axon polarity index, axon-tip/dendrite index, and PAEZ and AIS areas, also was performed using ImageJ version 1.44o, as detailed in the Supplemental Experimental Procedures.

Live-Cell Imaging

For imaging of TfR-GFP-containing vesicles (including both somatodendritic carriers and endosomes), neurons were transfected with plasmids encoding TfR-GFP on DIV4–DIV5. At DIV10, neurons were stained with CF555-conjugated antibody to NF for 30 min at 37°C. Cells were imaged on a spinning-disk confocal microscope (Marianas, Intelligent Imaging) equipped with a 63 \times 1.4 NA objective. Digital images were acquired with an EM-CCD camera (Evolve, Photometrics). For dual-color videos, TfR-GFP and NF-CF555 channels were sequentially exposed for 200 and 100 ms, respectively. Neurons were recorded every 500 ms for 120 s. PB was performed after ~5 s of video recording to facilitate identification of individual vesicle tracks.

For imaging of somatodendritic carrier vesicles emanating from the TGN, neurons were transfected with a bicistronic expression plasmid encoding Streptavidin-KDEL and TfR-SBP-GFP on DIV6–DIV7 and analyzed after 16–24 hr using the RUSH system (Boncompain et al., 2012). After transfection, neurons were maintained in Neurobasal medium without B27 supplement, because the presence of D-biotin in B27 interferes with the RUSH system. DIV7 neurons were incubated with 40 μ M D-biotin immediately before imaging on the spinning-disk confocal microscope. The release of TfR-SBP-GFP from the ER hook (Streptavidin-KDEL) was monitored under the microscope, and, after accumulation of TfR-SBP-GFP at the TGN (15–20 min after D-biotin addition), dual-color live-cell imaging was performed by sequential capture of 200-ms images of TfR-SBP-GFP and NF-CF555 every second for 120 s. A total of 15 neurons were analyzed.

For imaging of TfR-GFP-containing vesicles on DIV3 neurons cotransfected with control shRNA or AnkG shRNA and mCherry-tubulin, neurons were stained at DIV8 with CF640-conjugated antibody to NF and imaged on a

spinning-disk confocal microscope. Neurons were recorded every 500 ms for 120 s.

Quantification of live-cell imaging data and statistical analyses were performed as described in the [Supplemental Experimental Procedures](#).

Other Methods

Animal work was conducted under protocol 13-011 following United States regulations and guidelines set forth by the NIH, the Animal Welfare Act, the Guide for the Care and Use of Laboratory Animals, the Public Health Service Policy on Humane Care and Use of Laboratory Animals, and the Government Principles for the Utilization and Care of Vertebrate Animals Used in Testing, Research and Training. Additional methods and reagents are described in the [Supplemental Experimental Procedures](#).

SUPPLEMENTAL INFORMATION

Supplemental Information includes Supplemental Experimental Procedures, seven figures, and three movies and can be found with this article online at <http://dx.doi.org/10.1016/j.celrep.2015.09.074>.

ACKNOWLEDGMENTS

We thank K.E. Howell, P.J. Kammermeier, M. Komada, J. Lippincott-Schwartz, F. Perez, T.A. Rapoport, K.J. Verhey, and S. Vicini for gifts of reagents; X. Zhu and N. Tsai for technical assistance; and D.C. Gershlick for critical review of the manuscript. This work was funded by the Intramural Program of NICHD, NIH (ZIA HD001607).

Received: December 14, 2014

Revised: August 19, 2015

Accepted: September 24, 2015

Published: October 29, 2015

REFERENCES

- Aizawa, H., Sekine, Y., Takemura, R., Zhang, Z., Nangaku, M., and Hirokawa, N. (1992). Kinesin family in murine central nervous system. *J. Cell Biol.* *119*, 1287–1296.
- Al-Bassam, S., Xu, M., Wandless, T.J., and Arnold, D.B. (2012). Differential trafficking of transport vesicles contributes to the localization of dendritic proteins. *Cell Rep.* *2*, 89–100.
- Ango, F., di Cristo, G., Higashiyama, H., Bennett, V., Wu, P., and Huang, Z.J. (2004). Ankyrin-based subcellular gradient of neurofascin, an immunoglobulin family protein, directs GABAergic innervation at purkinje axon initial segment. *Cell* *119*, 257–272.
- Atherton, J., Houdusse, A., and Moores, C. (2013). MAPping out distribution routes for kinesin couriers. *Biol. Cell* *105*, 465–487.
- Baas, P.W., Deitch, J.S., Black, M.M., and Banker, G.A. (1988). Polarity orientation of microtubules in hippocampal neurons: uniformity in the axon and nonuniformity in the dendrite. *Proc. Natl. Acad. Sci. USA* *85*, 8335–8339.
- Berghs, S., Aggujaro, D., Dirx, R., Jr., Maksimova, E., Stabach, P., Hermel, J.M., Zhang, J.P., Philbrick, W., Slepnev, V., Ort, T., and Solimena, M. (2000). betaIV spectrin, a new spectrin localized at axon initial segments and nodes of ranvier in the central and peripheral nervous system. *J. Cell Biol.* *151*, 985–1002.
- Boncompain, G., Divoux, S., Gareil, N., de Forges, H., Lescure, A., Latreche, L., Mercanti, V., Jollivet, F., Raposo, G., and Perez, F. (2012). Synchronization of secretory protein traffic in populations of cells. *Nat. Methods* *9*, 493–498.
- Brady, S.T. (1985). A novel brain ATPase with properties expected for the fast axonal transport motor. *Nature* *317*, 73–75.
- Braun, N., Schikorski, T., and Zimmermann, H. (1993). Cytoplasmic segregation and cytoskeletal organization in the electric catfish giant electromotoneuron with special reference to the axon hillock region. *Neuroscience* *52*, 745–756.
- Burton, P.R. (1988). Dendrites of mitral cell neurons contain microtubules of opposite polarity. *Brain Res.* *473*, 107–115.
- Cameron, P.L., Südhof, T.C., Jahn, R., and De Camilli, P. (1991). Colocalization of synaptophysin with transferrin receptors: implications for synaptic vesicle biogenesis. *J. Cell Biol.* *115*, 151–164.
- Chu, P.J., Rivera, J.F., and Arnold, D.B. (2006). A role for Kif17 in transport of Kv4.2. *J. Biol. Chem.* *281*, 365–373.
- Correia, S.S., Bassani, S., Brown, T.C., Lisé, M.F., Backos, D.S., El-Husseini, A., Passafaro, M., and Esteban, J.A. (2008). Motor protein-dependent transport of AMPA receptors into spines during long-term potentiation. *Nat. Neurosci.* *11*, 457–466.
- DeBoer, S.R., You, Y., Szodorai, A., Kaminska, A., Pigino, G., Nwabuisi, E., Wang, B., Estrada-Hernandez, T., Kins, S., Brady, S.T., and Morfini, G. (2008). Conventional kinesin holoenzymes are composed of heavy and light chain homodimers. *Biochemistry* *47*, 4535–4543.
- Dotti, C.G., Sullivan, C.A., and Banker, G.A. (1988). The establishment of polarity by hippocampal neurons in culture. *J. Neurosci.* *8*, 1454–1468.
- Dwyer, N.D., Adler, C.E., Crump, J.G., L'Etoile, N.D., and Bargmann, C.I. (2001). Polarized dendritic transport and the AP-1 mu1 clathrin adaptor UNC-101 localize odorant receptors to olfactory cilia. *Neuron* *31*, 277–287.
- Fariás, G.G., Cuitino, L., Guo, X., Ren, X., Jamik, M., Mattera, R., and Bonifacino, J.S. (2012). Signal-mediated, AP-1/clathrin-dependent sorting of transmembrane receptors to the somatodendritic domain of hippocampal neurons. *Neuron* *75*, 810–823.
- Ferreira, A., Cáceres, A., and Kosik, K.S. (1993). Intraneuronal compartments of the amyloid precursor protein. *J. Neurosci.* *13*, 3112–3123.
- Galiano, M.R., Jha, S., Ho, T.S., Zhang, C., Ogawa, Y., Chang, K.J., Stanke-wich, M.C., Mohler, P.J., and Rasband, M.N. (2012). A distal axonal cytoskeleton forms an intra-axonal boundary that controls axon initial segment assembly. *Cell* *149*, 1125–1139.
- Garrido, J.J., Giraud, P., Carlier, E., Fernandes, F., Moussif, A., Fache, M.P., Debanne, D., and Dargent, B. (2003). A targeting motif involved in sodium channel clustering at the axonal initial segment. *Science* *300*, 2091–2094.
- Gauger, A.K., and Goldstein, L.S. (1993). The Drosophila kinesin light chain. Primary structure and interaction with kinesin heavy chain. *J. Biol. Chem.* *268*, 13657–13666.
- Gindhart, J.G.J., Jr., and Goldstein, L.S. (1996). Tetratricopeptide repeats are present in the kinesin light chain. *Trends Biochem. Sci.* *21*, 52–53.
- Hammond, J.W., Huang, C.F., Kaech, S., Jacobson, C., Banker, G., and Verhey, K.J. (2010). Posttranslational modifications of tubulin and the polarized transport of kinesin-1 in neurons. *Mol. Biol. Cell* *21*, 572–583.
- Hedstrom, K.L., Xu, X., Ogawa, Y., Frischknecht, R., Seidenbecher, C.I., Shrager, P., and Rasband, M.N. (2007). Neurofascin assembles a specialized extracellular matrix at the axon initial segment. *J. Cell Biol.* *178*, 875–886.
- Hedstrom, K.L., Ogawa, Y., and Rasband, M.N. (2008). AnkyrinG is required for maintenance of the axon initial segment and neuronal polarity. *J. Cell Biol.* *183*, 635–640.
- Held, H. (1895). Beiträge zur Structure der Nervenzellen und ihrer Vortsätze, Chapter 396–416 (*Arch. Anat. Physiol. Anat.*).
- Hirokawa, N., Pfister, K.K., Yorifuji, H., Wagner, M.C., Brady, S.T., and Bloom, G.S. (1989). Submolecular domains of bovine brain kinesin identified by electron microscopy and monoclonal antibody decoration. *Cell* *56*, 867–878.
- Huang, C.F., and Banker, G. (2012). The translocation selectivity of the kinesins that mediate neuronal organelle transport. *Traffic* *13*, 549–564.
- Hurd, D.D., and Saxton, W.M. (1996). Kinesin mutations cause motor neuron disease phenotypes by disrupting fast axonal transport in Drosophila. *Genetics* *144*, 1075–1085.
- Jain, S., Fariás, G.G., and Bonifacino, J.S. (2015). Polarized sorting of the cop-transporter ATP7B in neurons mediated by recognition of a dileucine signal by AP-1. *Mol. Biol. Cell* *26*, 218–228.

- Jenkins, S.M., and Bennett, V. (2001). Ankyrin-G coordinates assembly of the spectrin-based membrane skeleton, voltage-gated sodium channels, and L1 CAMs at Purkinje neuron initial segments. *J. Cell Biol.* *155*, 739–746.
- Jenkins, B., Decker, H., Bentley, M., Luisi, J., and Banker, G. (2012). A novel split kinesin assay identifies motor proteins that interact with distinct vesicle populations. *J. Cell Biol.* *198*, 749–761.
- Jones, S.L., Korobova, F., and Svitkina, T. (2014). Axon initial segment cytoskeleton comprises a multiprotein submembranous coat containing sparse actin filaments. *J. Cell Biol.* *205*, 67–81.
- Kaech, S., and Banker, G. (2006). Culturing hippocampal neurons. *Nat. Protoc.* *1*, 2406–2415.
- Kamal, A., Stokin, G.B., Yang, Z., Xia, C.H., and Goldstein, L.S. (2000). Axonal transport of amyloid precursor protein is mediated by direct binding to the kinesin light chain subunit of kinesin-I. *Neuron* *28*, 449–459.
- Kapitein, L.C., and Hoogenraad, C.C. (2011). Which way to go? Cytoskeletal organization and polarized transport in neurons. *Mol. Cell. Neurosci.* *46*, 9–20.
- Kapitein, L.C., Schlager, M.A., van der Zwan, W.A., Wulf, P.S., Keijzer, N., and Hoogenraad, C.C. (2010). Probing intracellular motor protein activity using an inducible cargo trafficking assay. *Biophys. J.* *99*, 2143–2152.
- Kobayashi, T., Storrie, B., Simons, K., and Dotti, C.G. (1992). A functional barrier to movement of lipids in polarized neurons. *Nature* *359*, 647–650.
- Kordeli, E., Lambert, S., and Bennett, V. (1995). AnkyrinG. A new ankyrin gene with neural-specific isoforms localized at the axonal initial segment and node of Ranvier. *J. Biol. Chem.* *270*, 2352–2359.
- Lasiecka, Z.M., and Winckler, B. (2011). Mechanisms of polarized membrane trafficking in neurons – focusing in endosomes. *Mol. Cell. Neurosci.* *48*, 278–287.
- Lavezzari, G., McCallum, J., Lee, R., and Roche, K.W. (2003). Differential binding of the AP-2 adaptor complex and PSD-95 to the C-terminus of the NMDA receptor subunit NR2B regulates surface expression. *Neuropharmacology* *45*, 729–737.
- Lewis, T.L.J., Jr., Mao, T., Svoboda, K., and Arnold, D.B. (2009). Myosin-dependent targeting of transmembrane proteins to neuronal dendrites. *Nat. Neurosci.* *12*, 568–576.
- Liao, G., and Gundersen, G.G. (1998). Kinesin is a candidate for cross-bridging microtubules and intermediate filaments. Selective binding of kinesin to detyrosinated tubulin and vimentin. *J. Biol. Chem.* *273*, 9797–9803.
- Luby-Phelps, K., Castle, P.E., Taylor, D.L., and Lanni, F. (1987). Hindered diffusion of inert tracer particles in the cytoplasm of mouse 3T3 cells. *Proc. Natl. Acad. Sci. USA* *84*, 4910–4913.
- Margeta, M.A., Wang, G.J., and Shen, K. (2009). Clathrin adaptor AP-1 complex excludes multiple postsynaptic receptors from axons in *C. elegans*. *Proc. Natl. Acad. Sci. USA* *106*, 1632–1637.
- Mattera, R., Farias, G.G., Mardones, G.A., and Bonifacio, J.S. (2014). Co-assembly of viral envelope glycoproteins regulates their polarized sorting in neurons. *PLoS Pathog.* *10*, e1004107.
- Maycox, P.R., Link, E., Reetz, A., Morris, S.A., and Jahn, R. (1992). Clathrin-coated vesicles in nervous tissue are involved primarily in synaptic vesicle recycling. *J. Cell Biol.* *118*, 1379–1388.
- Nakada, C., Ritchie, K., Oba, Y., Nakamura, M., Hotta, Y., Iino, R., Kasai, R.S., Yamaguchi, K., Fujiwara, T., and Kusumi, A. (2003). Accumulation of anchored proteins forms membrane diffusion barriers during neuronal polarization. *Nat. Cell Biol.* *5*, 626–632.
- Nakata, T., and Hirokawa, N. (2003). Microtubules provide directional cues for polarized axonal transport through interaction with kinesin motor head. *J. Cell Biol.* *162*, 1045–1055.
- Nakata, T., Niwa, S., Okada, Y., Perez, F., and Hirokawa, N. (2011). Preferential binding of a kinesin-1 motor to GTP-tubulin-rich microtubules underlies polarized vesicle transport. *J. Cell Biol.* *194*, 245–255.
- Palay, S.L., and Palade, G.E. (1955). The fine structure of neurons. *J. Biophys. Biochem. Cytol.* *1*, 69–88.
- Palay, S.L., Sotelo, C., Peters, A., and Orkand, P.M. (1968). The axon hillock and the initial segment. *J. Cell Biol.* *38*, 193–201.
- Pernigo, S., Lamprecht, A., Steiner, R.A., and Dodding, M.P. (2013). Structural basis for kinesin-1: cargo recognition. *Science* *340*, 356–359.
- Petersen, J.D., Kaech, S., and Banker, G. (2014). Selective microtubule-based transport of dendritic membrane proteins arises in concert with axon specification. *J. Neurosci.* *34*, 4135–4147.
- Pu, J., Schindler, C., Jia, R., Jamik, M., Backlund, P., and Bonifacio, J.S. (2015). BORC, a multisubunit complex that regulates lysosome positioning. *Dev. Cell* *33*, 176–188.
- Raine, C.S. (1999). Neurocellular anatomy. In *Basic Neurochemistry: Molecular, Cellular and Medical Aspects*, Sixth Edition, G.J. Siegel, B.W. Agranoff, R.W. Albers, S.K. Fisher, and M.D. Uhler, eds. (Philadelphia: Lippincott-Raven), pp. 3–30.
- Reed, N.A., Cai, D., Blasius, T.L., Jih, G.T., Meyhofer, E., Gaertig, J., and Verhey, K.J. (2006). Microtubule acetylation promotes kinesin-1 binding and transport. *Curr. Biol.* *16*, 2166–2172.
- Setou, M., Nakagawa, T., Seog, D.H., and Hirokawa, N. (2000). Kinesin superfamily motor protein KIF17 and mLin-10 in NMDA receptor-containing vesicle transport. *Science* *288*, 1796–1802.
- Sobotzik, J.M., Sie, J.M., Politi, C., Del Turco, D., Bennett, V., Deller, T., and Schultz, C. (2009). AnkyrinG is required to maintain axo-dendritic polarity in vivo. *Proc. Natl. Acad. Sci. USA* *106*, 17564–17569.
- Song, A.H., Wang, D., Chen, G., Li, Y., Luo, J., Duan, S., and Poo, M.M. (2009). A selective filter for cytoplasmic transport at the axon initial segment. *Cell* *136*, 1148–1160.
- Vale, R.D., Reese, T.S., and Sheetz, M.P. (1985). Identification of a novel force-generating protein, kinesin, involved in microtubule-based motility. *Cell* *42*, 39–50.
- Verhey, K.J., Meyer, D., Deehan, R., Blenis, J., Schnapp, B.J., Rapoport, T.A., and Margolis, B. (2001). Cargo of kinesin identified as JIP scaffolding proteins and associated signaling molecules. *J. Cell Biol.* *152*, 959–970.
- Watanabe, K., Al-Bassam, S., Miyazaki, Y., Wandless, T.J., Webster, P., and Arnold, D.B. (2012). Networks of polarized actin filaments in the axon initial segment provide a mechanism for sorting axonal and dendritic proteins. *Cell Rep.* *2*, 1546–1553.
- Winckler, B., Forscher, P., and Mellman, I. (1999). A diffusion barrier maintains distribution of membrane proteins in polarized neurons. *Nature* *397*, 698–701.
- Xu, K., Zhong, G., and Zhuang, X. (2013). Actin, spectrin, and associated proteins form a periodic cytoskeletal structure in axons. *Science* *339*, 452–456.
- Zheng, Y., Wildonger, J., Ye, B., Zhang, Y., Kita, A., Younger, S.H., Zimmerman, S., Jan, L.Y., and Jan, Y.N. (2008). Dynein is required for polarized dendritic transport and uniform microtubule orientation in axons. *Nat. Cell Biol.* *10*, 1172–1180.

Cell Reports

Supplemental Information

Sorting of Dendritic and Axonal Vesicles

at the Pre-axonal Exclusion Zone

Ginny G. Farías, Carlos M. Guardia, Dylan J. Britt, Xiaoli Guo, and Juan S. Bonifacino

Figure S1

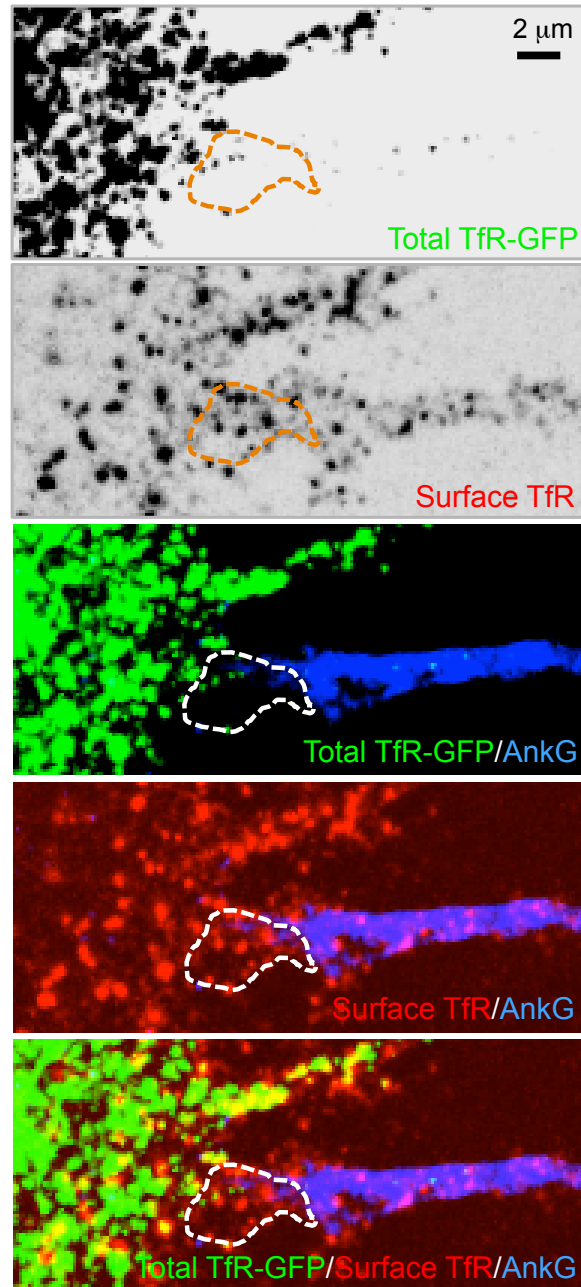


Figure S2

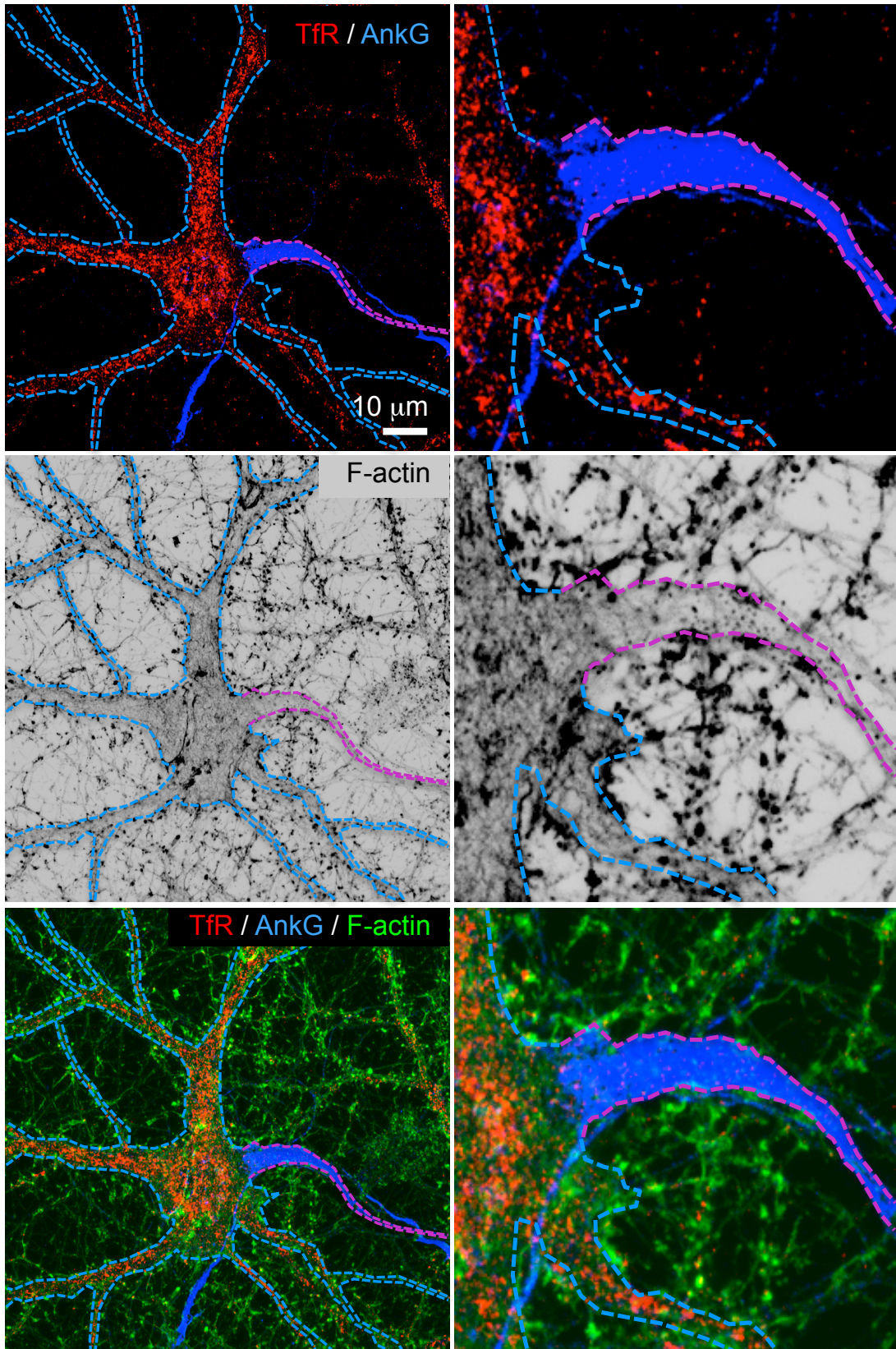


Figure S3

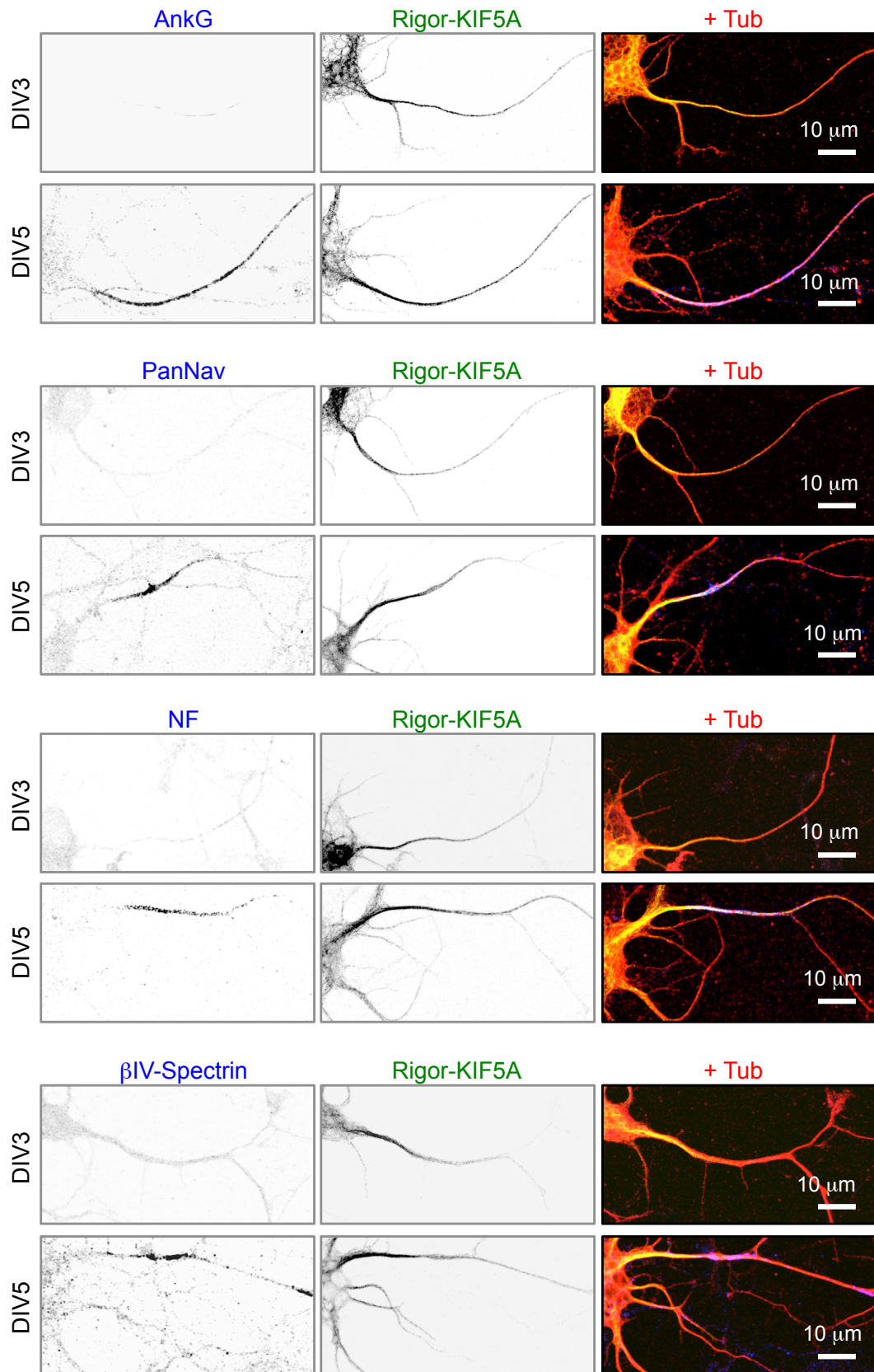


Figure S4

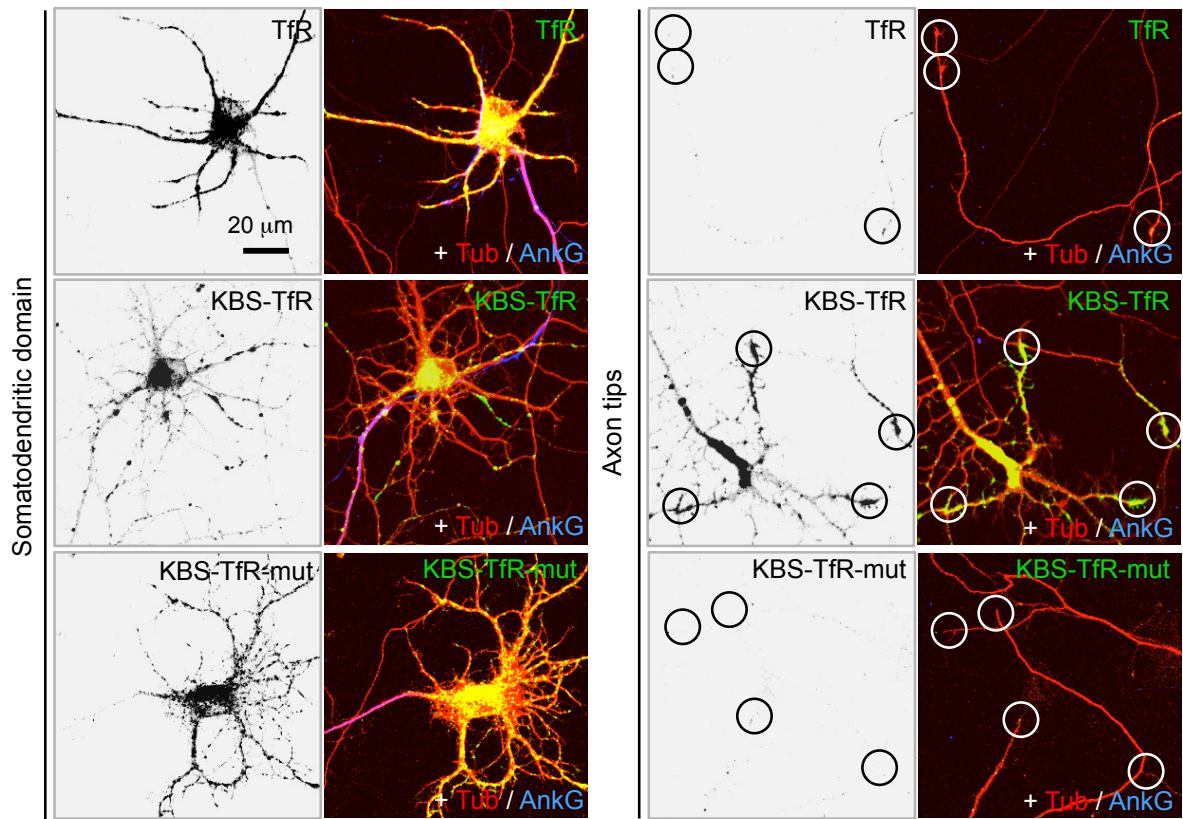


Figure S5

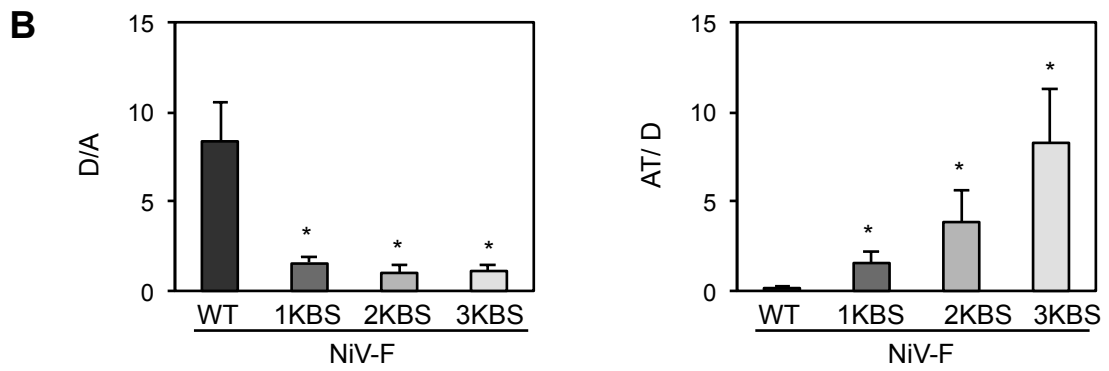
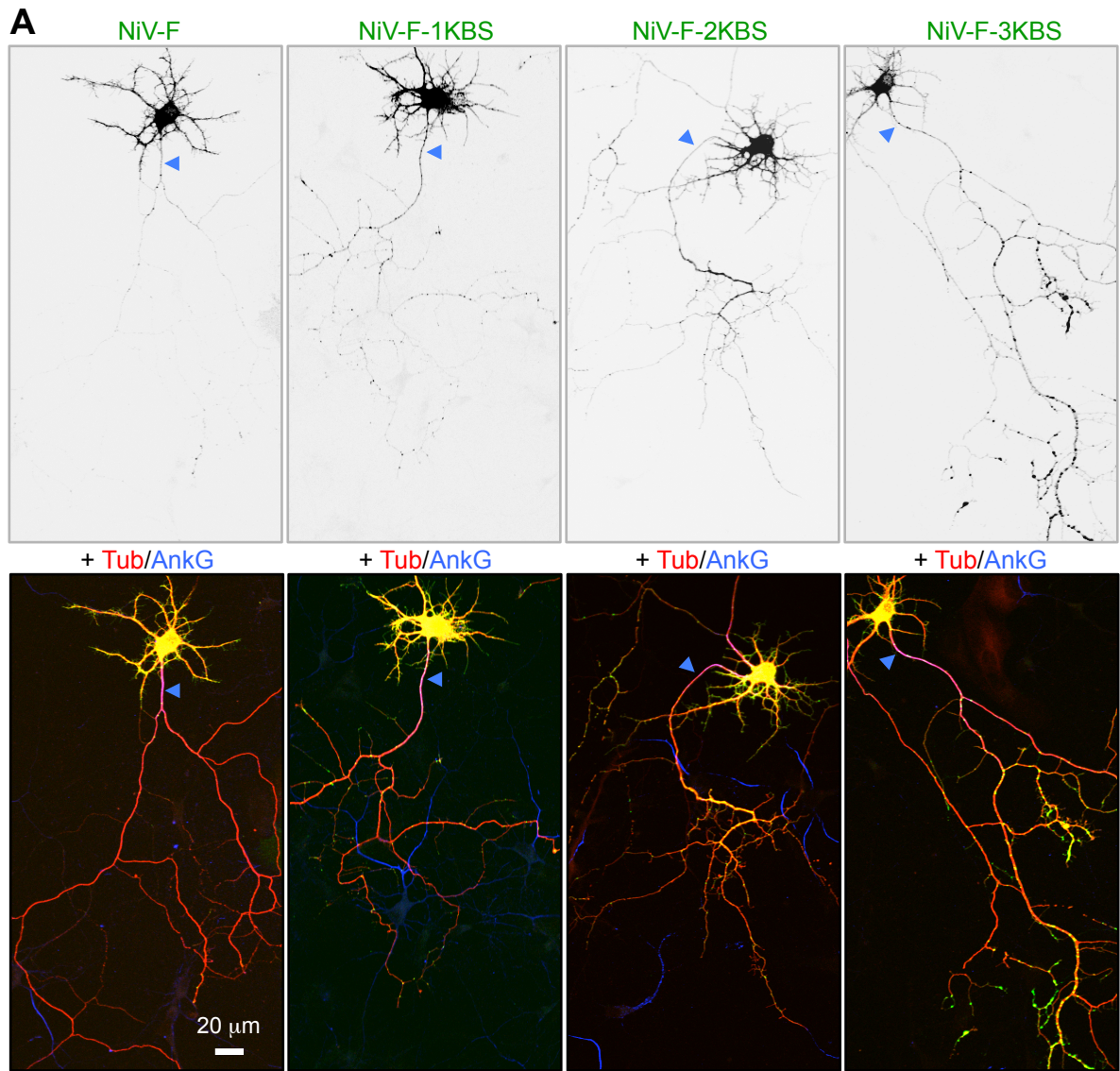


Figure S6

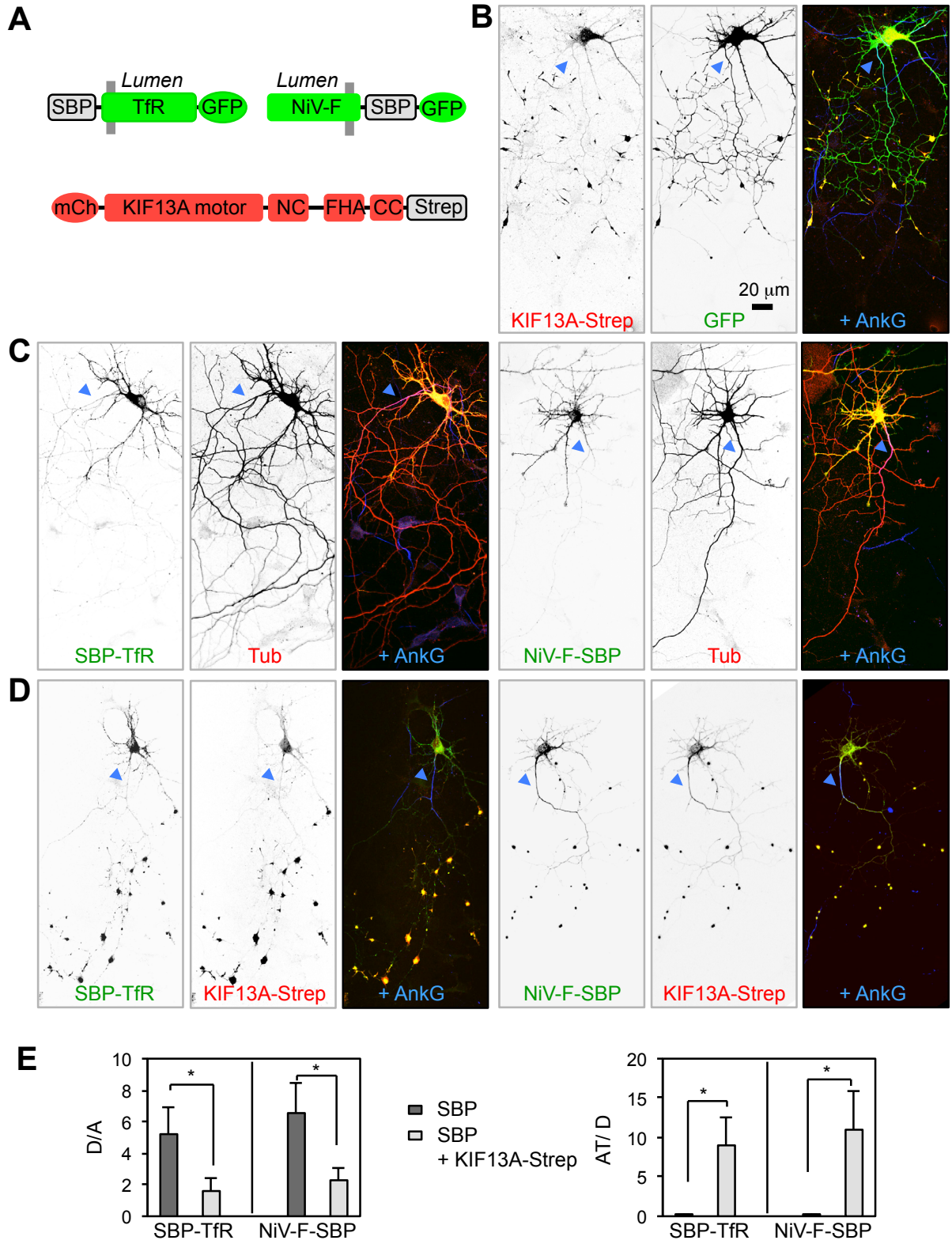
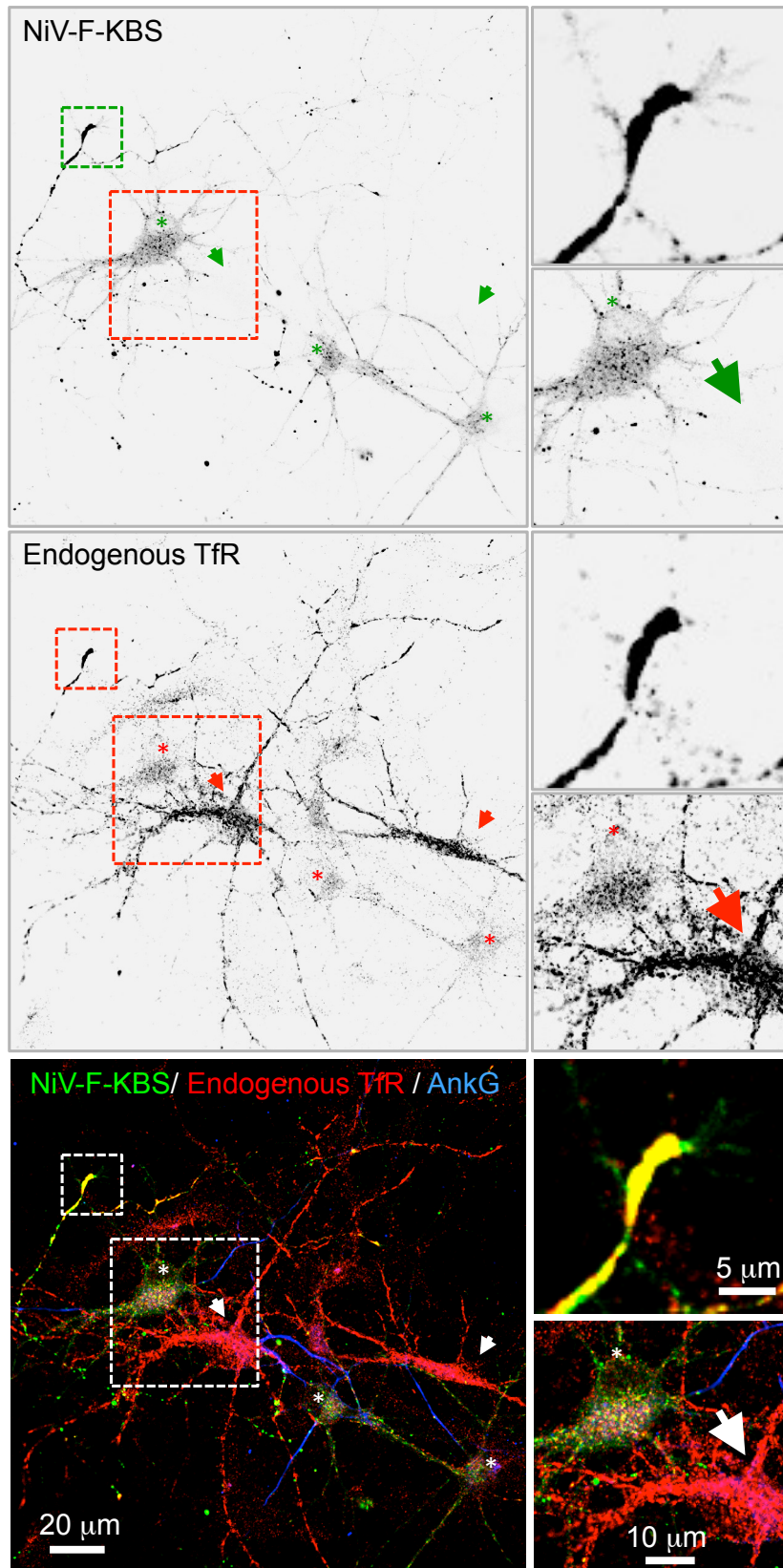


Figure S7



SUPPLEMENTAL FIGURE LEGENDS

Figure S1 (related to Figure 4). Surface TfR is not excluded from the plasma membrane of the PAEZ. DIV10 neurons transfected with a plasmid encoding TfR-GFP (grayscale and green) were stained for surface TfR by incubation of non-permeabilized cells with an antibody to GFP (grayscale and red) and, after fixation-permeabilization, for AnkG (blue) followed by appropriate secondary antibodies. Dashed lines indicate the PAEZ. The punctate staining of surface TfR reflects its localization to clathrin-coated pits.

Figure S2 (related to Figure 4). Absence of dense actin staining at the AIS in mature neurons. Z-stack reconstruction of DIV18 neurons stained for endogenous TfR (red), AnkG (blue) and F-actin (grayscale and green). Enlarged regions are shown on the right panels. Cyan and magenta dashed lines delimit the somatodendritic and axonal areas respectively. Notice the absence of a dense actin structure in the AIS.

Figure S3 (related to Figure 4). Rigor-KIF5A is preferentially recruited to the beginning of axonal microtubules prior to the assembly of the AIS. DIV3 and DIV5 neurons co-expressing GFP-Rigor-KIF5A (grayscale and green) and mCherry-tubulin (Tub) (red) stained for the AIS markers AnkG, PanNav, NF or β IV-Spectrin (grayscale and blue). Notice the preferential binding of Rigor-KIF5A to microtubules directed toward the axon as compared to dendrites before (DIV3) and after (DIV5) assembly of the AIS.

Figure S4 (related to Figure 5). Fusion of a kinesin-light-chain-binding sequence (KBS) to the TfR causes missorting of the chimera to the axon. Enlarged views of the somatodendritic domain (left panels) and axon tips (right panels) corresponding to the neurons in Figure 5B expressing TfR-GFP (upper panels), KBS-TfR-GFP (middle panels) and

KBS-TfR-mut-GFP (bottom panels) in grayscale/green. mCherry-tubulin (Tub) (red) expressed in the same cells was used to highlight both dendrites and axon, and endogenous AnkG staining (blue; appearing magenta in the merged images) to identify the AIS. Axon tips are indicated with circles.

Figure S5 (related to Figure 5). Effect of KBS copy number on missorting of NiV-F-KBS chimeras to the axon. (A) DIV7 neurons co-expressing NiV-F-GFP or NiV-F-KBS-GFP with one, two or three copies of the KBS sequence (grayscale in top row, green in bottom row) and mCherry-tubulin (Tub) (red) were immunostained for AnkG (blue; appearing as magenta in the merged images). Arrowheads point to the AIS. (B) Dendrite/axon (D/A) and axon tip/dendrite (AT/D) ratios of wild-type (WT) NiV-F and NiV-F with one, two or three copies of the KBS sequence. Values are the mean \pm SD from 20 neurons. * $P < 0.001$ relative to WT NiV-F.

Figure S6 (related to Figure 5). Forced interaction with KIF13A redirects SBP-TfR-GFP and NiV-F-SBP-GFP chimeras to the axon.

(A) A streptavidin-binding peptide (SBP) sequence (DEKTTGWRGGHVVEGLAGELEQLRARLEHHPQGQREP) was fused to the cytosolic N-terminus of TfR or C-terminus of NiV-F, both tagged with green fluorescent protein (GFP). Streptavidin (Strep) was fused to the C-terminus of a KIF13A₁₋₆₃₉ fragment comprising the motor, neck coil (NC) and forkhead-associated (FHA) domains plus part of the first coiled coil domain (CC) and tagged at the N-terminus with mCherry. (B) mCherry-KIF13A-Strep (red) distributes to axon tips in DIV7 neurons co-expressing soluble GFP (green). (C) SBP-TfR-GFP (green, left panels) and NiV-F-SBP-GFP (green, right panels) localize to the somatodendritic domain in DIV7 neurons co-expressing mCherry-tubulin (Tub) (red). (D) SBP-TfR-GFP (green, left panels) and NiV-F-SBP-GFP (green, right panels) are redirected to axon tips when co-expressed with mCherry-KIF13A-Strep (red). (B-D) Arrowheads point to

the AIS stained for AnkG (blue). (E) Dendrite/axon (D/A) and axon tip/dendrite (AT/D) ratios of SBP-TfR-GFP and NiV-F-SBP-GFP proteins in neurons co-expressing mCherry-tubulin or mCherry-KIF13A-Strep were quantified from 15 neurons and expressed as mean \pm SD. * $P < 0.001$.

Figure S7 (related to Figure 6). NiV-F-KBS chimera redirects endogenous TfR to axon tips.

DIV10 neurons expressing NiV-F-KBS-GFP (grayscale in upper panels; green in bottom panels) were stained for endogenous TfR (grayscale in middle panels; red in bottom panels) and AnkG (blue in bottom panels). Transfected and untransfected neurons are indicated by asterisks and arrows, respectively. Enlarged regions of an axon tip and soma are shown at the right of each image. Notice that NiV-F-KBS expression causes somatodendritic depletion of endogenous TfR and its accumulation at axon tips.

MOVIE LEGENDS

Movie S1 (related to Figure 2). Axonal exclusion of TfR-GFP-containing anterograde vesicles occurs at the PAEZ. DIV10 neuron expressing TfR-GFP (grayscale on the left panel, green on the right panel) was stained for the AIS with CF555-conjugated antibody to neurofascin (NF) (red on the right panel) and recorded every 500 ms for 120 s. Photobleaching (indicated as PB) was performed after ~5 s of recording to facilitate identification of vesicles entering an axon and a neighboring dendrite. Notice that few TfR-GFP-containing vesicles enter the PAEZ, while many enter the neighboring dendrite. Dendrite (D) and axon (A) are indicated.

Movie S2 (related to Figure 2). Vesicles budding from the Golgi complex enter the dendrites but not the PAEZ. DIV7 neuron co-expressing the ER-hook (Streptavidin-KDEL) and TfR-SBP-GFP (grayscale on the left panel, green on the right panel) and stained for the AIS with CF555-conjugated antibody to neurofascin (NF) (red on the right panel) was incubated with D-biotin for 20 min to release TfR-SBP-GFP from the ER-hook and allow for concentration at the Golgi complex. Cells were then recorded every second for 120 s. The AIS and PAEZ are indicated. Colored arrowheads on the grayscale image trace the trajectories of particles budding from the Golgi complex and moving into dendrites. Notice that most TfR-SBP-GFP vesicles budding from the Golgi complex enter dendrites but not the PAEZ.

Movie S3 (related to Figure 3). Axonal exclusion of somatodendritic vesicles in the absence of the AIS. DIV3 neurons co-transfected with control shRNA or AnkG shRNA together with TfR-GFP (grayscale) and mCherry tubulin (Tub) (red) were stained on DIV8 for the AIS with CF640-conjugated antibody to neurofascin (NF) (blue) to identify neurons expressing AnkG shRNA. Neurons were recorded for TfR-GFP every 500 ms for 120 s. DIV8 neuron expressing control shRNA (left, upper panels) and AnkG shRNA (left, bottom panels) and the respective

enlarged images from axon and dendrites (right panels). Notice that most TfR-GFP vesicles do not enter to the axon in absence of the AIS.

SUPPLEMENTAL EXPERIMENTAL PROCEDURES

Animals

Sprague-Dawley rats (Harlan Laboratories) were temporarily kept at the NIH animal facility. Animal work was conducted under protocol #13-011 following United States regulations and guidelines set forth by the NIH, the Animal Welfare Act, the Guide for the Care and Use of Laboratory Animals, the Public Health Service Policy on Humane Care and Use of Laboratory Animals and the Government Principles for the Utilization and Care of Vertebrate Animals used in Testing, Research and Training.

DNA constructs

Mouse KIF5A cDNA was cloned into pEGFP-C1 (Clontech). Human TfR and NiV-F cDNAs were cloned into pGFP(A206K)-N1 (Clontech), encoding a monomeric GFP variant, as previously described (Farías et al., 2012; Mattera et al., 2014). For construction of KBS-TfR and NiV-F-KBS, sequences encoding one, two or three copies of the kinesin-binding sequence (KBS) TNLEWDDSAI from SKIP (Pernigo et al., 2013; Pu et al., 2015) with a Gly residue between each copy were fused to sequences encoding the cytosolic N-terminus of TfR or C-terminus of NiV-F. Constructs were cloned into the pEGFP-N1 and pmCh-N1 vectors (Clontech). A bicistronic expression plasmid encoding the ER hook (Streptavidin-KDEL; streptavidin fused to a C-terminal ER retention signal Lys-Asp-Glu-Leu) and the reporter ManII-SBP-GFP (Boncompain et al., 2012) were gifts from F. Perez (Institut Curie, Paris, France). TfR-encoding sequences were cloned to replace ManII-encoding sequences in this vector.

For the forced interaction of TfR and NiV-F with KIF13A, sequences encoding a streptavidin-binding peptide (SBP) appended to the N-terminus of TfR or C-terminus of NiV-F were cloned into EGFP(A206K)-N1 (Clontech). An mCherry (mCh)-KIF13A-Strep chimera was generated by cloning sequences encoding the human KIF13A₁₋₆₃₉ fragment

(comprising the motor, neck coil, forkhead-associated and part of the first coiled-coil domain) (Soppina et al., 2014) and streptavidin into the pmCh-C1 vector (Clontech). A 6x(glycine-serine) linker was introduced between the KIF13A and streptavidin sequences to allow freedom of movement between domains. Plasmids encoding other proteins and their sources (in parenthesis) are: AnkG shRNA and control shRNA (Qiagen), mCherry-tubulin and TfR-mCherry (J. Lippincott-Schwartz, NIH, Bethesda, MD); RFP-CLIMP-63 and GFP-RTN (T. Rapoport, Harvard Medical School, Boston, MA); KLC-TPR-HA (K. Verhey, University of Michigan, Ann Arbor, MI); mGluR1-GFP (P. Kammermeier, University of Rochester Medical Center, Rochester, NY); NR2A-GFP (S. Vicini, Georgetown University Medical Center, Washington DC). Amino-acid substitutions in KIF5A-GFP (G235/A) (Rigor-KIF5A), KBS-TfR-GFP (KBS WD/AA), NiV-F-KBS-mCh (KBS WD/AA) and mCherry-tubulin (K40Q) were made by site-directed mutagenesis (QuikChange, Agilent) and verified by DNA sequencing.

Antibodies and other reagents

Rabbit anti-TfR (used at 1:200) and rabbit anti-GM130 (used at 1: 500) were from Abcam. Mouse anti-acetylated tubulin (used at 1:2000) and mouse anti-polyglutamylated tubulin (used at 1:1000) were from Sigma-Aldrich. Mouse anti-AP-1- γ (used at 1:300) and mouse anti-AP-2- α (used at 1:300) were from BD Transduction Laboratories. Goat anti-AnkG (used at 1:50) and rabbit anti-MAP2 (used at 1:300) were from Santa Cruz Biotechnology. Rabbit anti-GluR1 (used at 1:200) was from Millipore Bioscience Research Reagents. Mouse anti-HA (used at 1:1000) was from Covance. Mouse anti-pan-neurofascin (external), Clone A12/18 (used at 1:50), was from the University of California, Davis/NIH NeuroMab Facility. Mouse anti-NgCAM, Clone 8D9 (used at 1:300) made by V. Lemmon was obtained from the Developmental Studies Hybridoma Bank developed under the auspices of the NICHD and maintained by the University of Iowa, Department of Biology, Iowa, IA. Mouse anti-TGN38 (used at 1:500) was a gift from K. Howell, University of Colorado School of Medicine,

Denver, CO. Chicken anti- β IV-spectrin (used at 1:500) was a gift from M. Komada, Tokyo Institute of Technology, Tokyo, Japan. Rabbit anti-GFP and mouse anti-GFP (used at 1:1000), LysoTracker-Red DND-99, MitoTracker-Red-FM, and all secondary antibodies were obtained from Invitrogen. Phalloidin-Alexa405 (used at 1:100), Mix-n-Stain-CF488, Mix-n-Stain-CF555 and Mix-n-Stain-CF640R were from Biotium. The latter three reagents were used to label the antibody to neurofascin. Mix-n-Stain-CF555 was also used to label GFP for the surface staining of TfR-GFP as per the manufacturer's instructions.

Image analysis of fluorescently-labeled cells

Fluorescence line intensity plots: The distribution of different proteins at the transitional zone from the soma (S) to the axon (A) or dendrites (D) was quantified along 1- μ m-wide lines running 10-25 μ m in S \rightarrow A and S \rightarrow D directions in 10-20 neurons. Representative images and their corresponding plots are shown in Figures 1B and 1C, Figure 2E and 2F and Figure 3A and 3B.

Polarity index. The dendrite/axon (D/A) polarity index was quantified as previously described (Farías et al., 2012; Mattera et al., 2014). Briefly, several one-pixel-wide lines were traced along three dendrites and one portion of the axon (not including the AIS) captured in each image. The mean intensities from the three dendrites were averaged and used to calculate the D/A ratio from a total of 25 neurons. D/A=1 represents non-polarized distribution; D/A>1, preferential dendritic localization; D/A<1, preferential axonal localization. For calculation of the D/A index of endogenous TfR shown in Figure 1E, AnkG immunostaining and phalloidin were used to mark the AIS and all neurites, respectively, except for DIV2-3, when the axon was identified as the longest neurite stained with phalloidin-Alexa405, because of the absence of AnkG expression (Figure 1F). For experiments using AnkG shRNA or control shRNA shown in Figure 3, one-pixel-wide lines were traced along the first 30 μ m of each axon stained for the AIS marker AnkG. Knocking down of AnkG was calculated from 20 neurons and expressed as percentage. The total and surface

TfR-GFP D/A indexes were calculated similarly to the endogenous TfR D / A polarity index from 20 neurons for each one. For experiments using chimeras shown in Figures 5, 6, 7, S4, S5 and S6 the D/A and axon-tips/dendrite (AT/D) indexes were calculated similarly to the endogenous TfR D/A polarity index. Several one-pixel-wide lines were traced along three axon tips and three dendrites corresponding to the same transfected neuron and averaged to calculate AT/D ratios for each neuron. A total of 15-25 neurons were quantified for each condition. AT/D ratio >1 represents axon tip accumulation; <1 preferential dendritic accumulation. Axon tips were identified by staining for endogenous polyglutamylated tubulin at the end of axons marked by mCh-tubulin expression.

AIS and PAEZ areas. To quantify the AIS area indicated in Figure 1E, the area stained for AnkG was delimited by freehand selection for each neuron. An average area was calculated from a total of 25 AIS corresponding to 25 different neurons. The PAEZ area shown in Figure 1E was calculated similarly to the AIS area, except that it was selected in merged images of TfR and AnkG staining as a zone devoid of both proteins. Because of the absence of AnkG at DIV2-3, it was not possible determine the area of the AIS and PAEZ at this stage of neuronal development in culture.

Quantification of live-cell imaging

Movement of particles containing TfR-GFP was quantified using ImageJ version 1.44o. Lines (20-pixel-wide, 35-mm-long) were traced from the soma to the axon (S→A) and from the soma to the dendrites (S→D) in photobleached regions from 15 neurons (as shown in Figure 2B). Kymographs were generated from straightened lines by re-slicing stacks followed by z-projection. (S→A) and (S→D) tracks were orientated so that anterograde movement occurred from left to right. The number of anterograde particles entering the dendrites and axons was determined manually from kymographs. Quantification of the number of particles moving from soma to axon was subdivided into the PAEZ and the AIS regions. The PAEZ was defined as a region 5- μ m proximal to the edge of the AIS stained by anti-NF-CF555. To

compare anterograde transport to the axon versus dendrites, the total number of particles (100 %) was considered to be [(S→PAEZ) + (S→AIS) + (S→D)]. The trajectory of particles entering the PAEZ/ AIS was monitored regardless of whether they stopped and returned to the soma or continued to distal parts of the axon. Anterograde movement followed by stoppage and retrograde transport to the soma was observed as loops in kymographs at the PAEZ (Figure 2C). The total number of particles analyzed is indicated in Figure 2H.

Anterograde transport of particles containing TfR-SBP-GFP from the TGN to axon and dendrites was determined manually. Because of the small number of particles budding from the TGN, three different S→D tracks were quantified and averaged to compare with the S→A track for each neuron. Quantification of the number of particles moving from soma to axon was subdivided into the PAEZ and the AIS and represented as percentage, similar to TfR-GFP vesicle transport described above. A total of 15 neurons were analyzed. The total number of particles (n) analyzed is indicated in Figure 2L.

Statistical Methods

All the pooled data are presented as the mean \pm SD or the percentage \pm SEM as indicated in each figure legend from at least three independent experiments. Two-tailed Student's t test for unpaired data was used to evaluate single comparisons between different experimental groups using Microsoft Excel. Differences were considered statistically significant for a value of $P < 0.001$. n.s. not significant.

SUPPLEMENTAL REFERENCES

- Boncompain, G., Divoux, S., Gareil, N., de Forges, H., Lescure, A., Latreche, L., Mercanti, V., Jollivet, F., Raposo, G., and Perez, F. (2012). Synchronization of secretory protein traffic in populations of cells. *Nat Methods* 9, 493-498.
- Farías, G. G., Cuitiño, L., Guo, X., Ren, X., Jarnik, M., Mattera, R., and Bonifacino, J. S. (2012). Signal-Mediated, AP-1/Clathrin-Dependent Sorting of Transmembrane Receptors to the Somatodendritic Domain of Hippocampal Neurons. *Neuron* 75, 810-823.
- Mattera, R., Farías, G. G., Mardones, G. A., and Bonifacino, J. S. (2014). Co-assembly of viral envelope glycoproteins regulates their polarized sorting in neurons. *PLoS Pathog* 10, e1004107.
- Pernigo, S., Lamprecht, A., Steiner, R. A., and Dodding, M. P. (2013). Structural basis for kinesin-1:cargo recognition. *Science* 340, 356-359.
- Pu, J., Schindler, C., Jia, R., Jarnik, M., Backlund, P., and Bonifacino, J. S. (2015). BORC, a multisubunit complex that regulates lysosome positioning. *Dev. Cell*, in press.
- Soppina, V., Norris, S.R., Dizaji, A.S., Kortus, M., Veatch, S., Peckham, M., Verhey, K.J. (2014) Dimerization of mammalian kinesin-3 motors results in superprocessive motion. *Proc Natl Acad Sci U S A*. 111, 5562-5567.